Journal of Inorganic Biochemistry 174 (2017) 63–75

Contents lists available at ScienceDirect

Journal of Inorganic Biochemistry

journal homepage: www.elsevier.com/locate/jinorgbio

New Cu(II) complexes with pyrazolyl derived Schiff base ligands: Synthesis and biological evaluation

Nádia Ribeiro[a], Somnath Roy[a,b], Nataliya Butenko[a,c], Isabel Cavaco[a,c], Teresa Pinheiro[d], Irina Alho[e], Fernanda Marques[f], Fernando Avecilla[g], João Costa Pessoa[a], Isabel Correia[a,*]

[a] Centro de Química Estrutural, Instituto Superior Técnico, Universidade de Lisboa, Av. Rovisco Pais, 1049-001 Lisboa, Portugal
[b] Department of Chemistry, Ananda Chandra College, Jalpaiguri, West Bengal, India
[c] Departamento de Química Bioquímica e Farmácia, Universidade do Algarve, Campus de Gambelas, 8005-139 Faro, Portugal
[d] Instituto de Bioengenharia e Biociências, Departamento de Engenharia e Ciências Nucleares, Instituto Superior Técnico, Universidade de Lisboa, Av. Rovisco Pais 1, 1049-001 Lisboa, Portugal
[e] Instituto de Medicina Molecular, Faculdade de Medicina, Universidade de Lisboa, Av. Professor Egas Moniz, 1649-028 Lisboa, Portugal
[f] Centro de Ciências e Tecnologias Nucleares, Instituto Superior Técnico, Universidade de Lisboa, Estrada Nacional 10, 2695-066 Bobadela LRS, Portugal
[g] Grupo Xenomar, Centro de Investigacións Científicas Avanzadas (CICA), Departamento de Química, Facultade de Ciencias, Universidade da Coruña, Campus de A Coruña, 15071 A Coruña, Spain

ARTICLE INFO

Keywords:
Pyrazole
Schiff base ligand
Copper complexes
Cytotoxicity
Fluorescence quenching

ABSTRACT

Since the discovery of *cisplatin* there has been a continuous pursuit for new metallodrugs showing higher efficacies and lower side effects. In this work, new copper(II) complexes (**C1–C6**) of Schiff bases derived from pyrazolyl were developed. Through condensation of 5-methyl-1*H*-pyrazole-3-carbohydrazide with different aromatic aldehydes – pyridoxal, salicylaldehyde, 3-methoxy-2-hydroxybenzaldehyde, 3-ethoxy-2-hydroxybenzaldehyde and 2-hydroxynaphthene-1-carbaldehyde – a set of new pyrazole based "ONO" tridentate Schiff bases were obtained in moderate to good yields – **L1–L6**, as well as their Cu(II)-complexes. All compounds were characterized by analytical techniques and their molecular formulae established. The antioxidant potential of all compounds was tested, yielding low activity in most cases, with the exception of **L1** and **C5**. The Cu(II) complexes were tested for their aqueous stability, and for their interaction with biological molecules, namely DNA and HSA (human serum albumin), through fluorescence quenching experiments (and electrophoresis for DNA). With the exception of **C3**, all the synthesized complexes were able to interact with DNA and HSA. Their cytotoxic activity against two cancer cell lines (MCF7 — breast and PC3 — prostate) was also evaluated. Complexes **C5** and **C6**, with larger aromatic systems, showed much higher cytotoxicity (in the low μM range), than **C1–C4**, as well as IC_{50} values much lower than *cisplatin*. For **C6** the results suggest that the mechanisms of cell death do not seem to be mediated by apoptosis, through caspases 3/7 activation, but by involving membrane potential and imbalance in physiological elements such as P, K and Ca.

1. Introduction

Cancer is one of the diseases with higher impact at personal, social and economic level [1]. It is nowadays the leading cause of death in economically developed countries and the second one in developing countries [2]. The common feature to all forms of cancer is high genomic instability; this leads to continuous acquisition of DNA aberrations, which prompt the cancer cells to adapt, resist, and become continuously more aggressive [2].

Among various types of anticancer drugs, metal-based complexes have been under much attention since the discovery of *cisplatin* in the 1960s [3]. The interest in developing coordination compounds of different metal ions for application as anticancer agents arises from the fact that platinum-based drugs, although possessing a powerful anticancer effect, present undesirable side-effects and are only efficient against a restricted variety of cancer cells. Also, the fact that platinum is an exogenous metal to the human organism can lead to a response from the body that can severely prejudice the efficacy of the drug and/or its toxic side effects can prevail over the therapeutic ones. There is, therefore, an interest in developing new drugs based in endogenous metal ions, such as copper, considered to have less side-effects, with improved spectrum of efficacy and lower toxicity [4], as well as affording distinct mechanisms of action. Copper is a trace element in the human body and acts as cofactor in enzymes and other structures,

* Corresponding author.
E-mail address: icorreia@tecnico.ulisboa.pt (I. Correia).

http://dx.doi.org/10.1016/j.jinorgbio.2017.05.011
Received 22 February 2017; Received in revised form 19 May 2017; Accepted 22 May 2017
Available online 01 June 2017
0162-0134/

making its presence indispensable for the normal function of the organism. It is therefore no surprise that compounds containing this element are being considered in the development of metallodrugs [5,6].

The use of copper complexes has, in many cases, the genetic material as primary target, the damage being provided by different mechanisms that can be promoted by intercalation of the compound into the DNA double helix [7]. The success of metal-based drugs is closely linked to the proper choice of the auxiliary ligand, which plays a key role in modifying reactivity, lipophilicity, and stabilizing specific oxidation states. Ligands containing nitrogen atoms have been widely used in coordination chemistry and, in particular, as elements for the synthesis and development of pharmaceuticals. Extensive research has been done using the simple chemistry that leads to the formation of Schiff bases [8]. One of the most interesting characteristics of Schiff bases is its modular character, since the combination of different amines with different aldehydes may yield compounds with different features. They exhibit a broad range of biological activities, including antifungal, antibacterial, antimalarial, antiproliferative, anti-inflammatory, antiviral, and antipyretic properties [8–11].

Schiff bases and their metal complexes in particular copper(II) complexes are important in drug research and development due to their bioactivity [1]. Interesting features among some of these complexes are the favourable DNA intercalative abilities, antiproliferative activity, dependence on the cell type and induction of apoptosis [11,12]. Pyrazoles and their derivatives are one important group of compounds in drug research. These consist of a doubly unsaturated 5-membered ring containing two nitrogen atoms (positions 1 and 2 of the ring) [13]. The attractiveness of pyrazole and its derivatives is their versatility that allows the synthesis of a series of analogues containing different moieties, thus affecting the electronics and by extension the properties of the resultant compounds [14]. The core pyrazole structure, in general, has attracted widespread attention also because of the diversity of biological activity shown by derivatives of this nucleus, such as antimicrobial, anticancer, cytotoxic, analgesic, anti-inflammatory, antihypertensive, central nervous system activity like antiepileptic, antidepressant, *etc.* [13,15]. Substitution with a carbohydrazide moiety at position C5 of the pyrazole ring provides derivatives that can undergo condensation with aldehydes, forming Schiff bases. These compounds also exhibit antitumour activity, particularly those resulting from the reaction with salicylaldehyde [15].

In this work we report the synthesis and characterization of new Schiff base complexes and analyze their interaction with biomolecules, such as DNA and Human Serum Albumin (HSA), as well as their potential anticancer activity. The choice fell on copper complexes with Schiff bases derived from pyrazole-3-carbohydrazide and aromatic substituents, such as pyridoxal, salicylaldehyde and its derivatives, and 2-hydroxynaphthene-1-carbaldehyde — see Scheme 1.

2. Experimental part

2.1. Materials

5-Methyl-1*H*-pyrazole-3-carbohydrazide, pyridoxal hydrochloride, 2-hydroxybenzaldehyde, 3-methoxy-2-hydroxybenzaldehyde, and 3-ethoxy-2-hydroxybenzaldehyde (all from Sigma) were used as received. The metal salt $CuCl_2{\cdot}2H_2O$ (Merck) was used as supplied. Methanol (Aldrich) and dimethyl sulfoxide (Carlo Erba) were p.a. grade and used without further purification. Millipore® water was used throughout all the experiments with biological macromolecules. Phosphate buffered saline (PBS) was purchased from Sigma-Aldrich as tablets readily soluble in water (deionized water) giving solutions 0.01 M in phosphate (and NaCl 0.138 M; KCl 0.0027 M), pH 7.4 at 25 °C. Calf thymus DNA (ctDNA), thiazole orange (TO) and Human Serum Albumin (HSA) (fatty acid free) were purchased from Sigma-Aldrich. All other materials not mentioned here were either p.a. or reagent grade.

2.2. Instrumentation

Elemental analysis for C, H and N were carried on a FISONS EA 1108 CHNS-O apparatus. The ^{1}H NMR spectra were recorded at ambient temperature on a Bruker Avance II + 300 (UltraShieldTM Magnet) spectrometer operating at 300.13 MHz. The chemical shifts are reported in ppm using tetramethylsilane as internal reference. The infrared spectra were recorded on a JASCO FT/IR 4100 spectrophotometer and the UV–Visible absorption spectra were recorded on a Perkin Elmer Lambda 35 UV–Vis spectrophotometer with 10.0 mm quartz cuvettes. A 500-MS Varian Ion Trap Mass Spectrometer was used to measure ESI-MS spectra of methanolic solutions of the complexes in both positive and negative modes. The first derivative X-band EPR spectra of the frozen solutions (frozen in liquid nitrogen, 77 K) were recorded on a Bruker ESP 300E spectrometer. The spectrometer was operated at ~9.51 GHz with a frequency modulation of 100 kHz. An ion chromatography system was used to determine the presence and amount of chloride using a DIONEX ICS-1500, equipped with IonPac® AS14A 4-mm analytical (4 × 250 mm) column and suppressed conductivity at 10 μSFS ASRS®-ULTRA AutoSuppression® recycle mode detection system. Fluorescence measurements were carried out on a SPEX® Fluorolog spectrofluorimeter (Horiba Jobin Yvon) in a FL3-11 configuration, equipped with a Xenon lamp and in a 10.0 mm quartz cuvette. The instrumental response was corrected by means of a correction function provided by the manufacturer. The experiments were carried out at room temperature and are all steady-state measurements.

2.3. Synthesis and characterization

2.3.1. Synthesis of the ligands

Ligands **L1** to **L5** were synthesized in by refluxing a methanolic solution (25 mL) of 5-methyl-1*H*-pyrazole-3-carbohydrazide (250 mg, 1.78 mmol) with the corresponding aldehyde (1.78 mmol), also taken in methanol (25 mL), for *ca.* 5 h in the presence of two drops of acetic acid. White to yellowish solid compounds separated out. They were filtered, washed with cold methanol and dried in vacuum. The general synthesis of the ligands is given in Scheme 1.

*2.3.1.1. (E)-N′-((3-hydroxy-5-(hydroxymethyl)-2-methylpyridin-4-yl)-5-methyl-1H-pyrazole-3-carbohydrazide hydrochloride (**L1**).* Yield: 83%; ESI-MS (electrospray ionization mass spectra) (MeOH) *m/z* [Found (Calcd)]: 290.1 (290.12) (100%) $[L + H]^+$; 288.6 (288.12) (15%) $[L - H]^-$; 324.2 (324.09) (100%) $[L + Cl]^-$; 612.9 (613.24) (80%) $[2L + Cl]^-$. *Anal.* Calc. for $C_{13}H_{16}ClN_5O_3$: C, 47.90; H, 4.95; N, 21.50. Found: C, 48.1; H, 4.9; N, 21.7%. FTIR (KBr, cm^{-1}): 3440 (m, pyr, $-CH_2OH$), 3338 (s, NH), 3204 (s, pyr, −OH), 2868 (s, pyr, $N-H^+-Cl^-$), 1658 (s, −C═O), 1599 (m, azomethine, C═N), 1562 (s, C═C), 1411 (m, pz, C═N). ^{1}H NMR (300 MHz, DMSO-d_6, δ (ppm)): 2.08 (s, 1H, pyr, $-CH_2O\mathbf{H}$), 2.31 (s, 3H, pz, $-CH_3$), 2.61 (s, 3H, pyr, $-CH_3$), 4.74 (s, 2H, pyr, $-C\mathbf{H_2}OH$), 6.62 (s, 1H, pz, −CH), 8.19 (s, 1H, pyr, −CH), 9.04 (s, 1H, −CH═N), 12.83 (s, 1H, NNH), 13.21 (s, 1H, pz, −NH). ^{13}C NMR (300 MHz, DMSO-d_6, δ (ppm)): 10.61 (pz, $-CH_3$), 14.79 (pyr, $-CH_3$), 58.18 (pyr, $-CH_2OH$), 105.85 (pz, −CH), 115.98, 129.70, 135.74, 151.87, 153.57 (pyridine moiety), 140.74, 147.99 (pyrazolyl moiety), 143.68 (−CH═N), 158.19 (carbonyl). UV–Vis [MeOH, λ_{max}/nm (ε/M^{-1} cm^{-1})]: 296 (1.55×10^4), 309 (1.98×10^4), 319 (1.96×10^4), 342 (1.81×10^4), 355 (1.61×10^4), 403 (5.01×10^2).

*2.3.1.2. (E)-N′-(2-hydroxybenzylidene)-5-methyl-1H-pyrazole-3-carbohydrazide (**L2**).* Yield: 85.7%; ESI-MS (MeOH) *m/z* [Found (Calcd)]: 245.2 (245.10) (100%) $[L + H]^+$; 243.8 (243.1) (95%) $[L - H]^-$. *Anal.* Calc. for $C_{12}H_{12}N_4O_2$: C, 59.01; H, 4.95; N, 22.94. Found: C, 59.1; H, 4.9; N, 22.6%. FTIR (KBr, cm^{-1}): 3281 (m, −N−NH), 3172 (m, −OH), 1683 (s, −C═O), 1649 (m, azomethine, C═N), 1545 (s, C═C), 1488 (m, pz, C═N). ^{1}H NMR (300 MHz, DMSO-

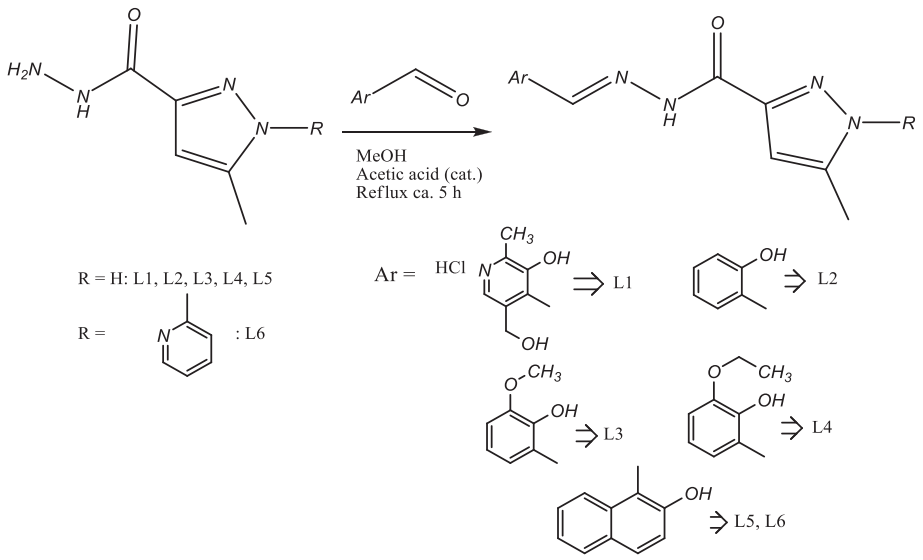

Scheme 1. General scheme for the synthesis of the ligands used in this work. The substituents chosen allow variation in steric hindrance, electron donating ability and aromaticity.

d_6, δ (ppm)): 2.30 (s, 3H, pz, −CH_3), 6.52 (s, 1H, pz, −CH), 6.94 (m, 2H, aromatic), 7.29 (m, 1H, aromatic), 7.43 (m, 1H, aromatic), 8.66 (s, 1H, −CH═N), 11.46 (s, 1H, −OH), 11.98 (s, 1H, pz, −NH), 13.14 (s, 1H, NNH). ^{13}C NMR (300 MHz, DMSO-d_6, δ (ppm)): 10.68 (pz, −CH_3), 105.35 (pz, −CH), 116.29, 118.66, 119.30, 129.73, 131.63, 157.40 (benzylidene moiety), 140.72, 148.13 (pyrazolyl moiety), 148.68 (−CH═N), 157.35 (carbonyl). UV–Vis [DMF, λ_{max}/nm (ε/M^{-1} cm^{-1})]: 276 (1.03 × 10^4), 286 (1.61 × 10^4), 297 (1.77 × 10^4), 325 (1.25 × 10^4), 332 (1.20 × 10^4).

*2.3.1.3. (E)-N′-(3-methoxy-2-hydroxybenzylidene)-5-methyl-1H-pyrazole-3-carbohydrazide (**L3**)*. Yield: 67.5%; ESI-MS (MeOH) *m/z* [Found (Calcd)]: 275.3 (275.11) (20%) [L + H]$^+$; 297.2 (297.11) (100%) [L + Na]$^+$; 570.8 (571.22) (55%) [2L + Na]$^+$; 273.3 (273.11) (100%) [L − H]$^-$. *Anal.* Calc. for $C_{13}H_{14}N_4O_3$: C, 56.93; H, 5.14; N, 20.43. Found: C, 56.8; H, 5.3; N, 20.4%. FTIR (KBr, cm^{-1}): 3302 (s, NH), 1666 (s, −C═O), 1610 (m, azomethine, C═N), 1542 (s, C═C), 1468 (s, pz, C═N). ^{1}H NMR (300 MHz, DMSO-d_6, δ (ppm)): 2.30 (s, 3H, pz, −CH_3), 3.81 (s, 3H, −OCH_3), 6.52 (s, 1H, pz, −CH), 6.85 (m, 1H, aromatic), 7.01 (m, 2H, aromatic), 8.66 (s, 1H, −CH═N), 11.24 (s, 1H, −OH), 11.96 (s, 1H, pz, −NH), 13.14 (s, 1H, NNH). ^{13}C NMR (300 MHz, DMSO-d_6, δ (ppm)): 10.67 (pz, −CH_3), 56.16 (−O**CH_3**), 105.35 (pz, −CH), 113.77, 118.84, 118.94, 121.36, 147.24, 147.92 (benzylidene moiety), 140.13, 145.43 (pyrazolyl moiety), 148.62 (−CH═N), 158.50 (carbonyl). UV–Vis [DMSO, λ_{max}/nm (ε/M^{-1} cm^{-1})]: 300 (2.72 × 10^4), 309 (2.55 × 10^4), 333 (1.05 × 10^4).

*2.3.1.4. (E)-N′-(3-ethoxy-2-hydroxybenzylidene)-5-methyl-1H-pyrazole-3-carbohydrazide (**L4**)*. Yield: 62%; ESI-MS (MeOH) *m/z* [Found (Calcd)]: 289.3 (289.12) (30%) [L + H]$^+$; 598.9 (599.24) (100%) [2 L + H]$^+$; 287.4 (287.12) (75%) [L − H]$^-$; 574.8 (575.24) (100%) [2L − H]$^-$. *Anal.* Calc. for $C_{14}H_{16}N_4O_3{\cdot}0.2H_2O$: C, 57.61; H, 5.66; N, 19.19. Found: C, 57.8; H, 5.7; N, 19.3%. FTIR (KBr, cm^{-1}): 3311 (w, −N−NH), 3253 (w, −OH), 1667 (s, −C═O), 1539 (s, C═C), 1467 (s, pz, C═N). ^{1}H NMR (300 MHz, DMSO-d_6, δ (ppm)): 1.34 (t, 3H, −OCH_2C**H_3**), 2.30 (s, 3H, pz, −CH_3), 4.07 (m, 2H, −O**CH_2**CH_3), 6.53 (s, 1H, pz, −CH), 6.83 (m, 1H, aromatic), 6.99 (m, 2H, aromatic), 8.66 (s, 1H, −CH═N), 11.28 (s, 1H, −OH), 11.97 (s, 1H, pz, −NH), 13.14 (s, 1H, NNH). ^{13}C NMR (300 MHz, DMSO-d_6, δ (ppm)): 10.38 (pz, –CH_3), 14.78 (−OCH_2**CH_3**), 64.19 (−O**CH_2**CH_3), 104.95 (pz, −CH), 115.25, 119.04, 121.37, 136.31, 145.37, 147.50 (benzylidene moiety), 140.21, 147.15 (pyrazolyl moiety), 148.32 (−CH═N), 158.22 (carbonyl). UV–Vis [DMSO, λ_{max}/nm (ε/M^{-1} cm^{-1})]: 300 (3.11 × 10^4), 310 (2.90 × 10^4), 341 (1.02 × 10^4).

*2.3.1.5. (E)-N′-((3-hydroxynaphthalen-1-yl) methylene)-5-methyl-1H-pyrazole-3-carbohydrazide (**L5**)*. Yield: 60.0%; ESI -MS (MeOH) *m/z* [Found (Calcd)]: 293.4 (293.11) (35%) [L − H]$^-$; 329.1 (329.08) (10%) [L + Cl]$^-$; 586.9 (587.22) (100%) [2L − H]$^-$. *Anal.* Calc. for $C_{16}H_{14}N_4O_2$: C, 65.30; H, 4.79; N, 19.04. Found: C, 65.1; H, 4.8; N, 18.7%. FTIR (KBr, cm^{-1}): 3196 (s, −N−NH), 3148 (s, −OH), 1671 (s, −C═O), 1626 (m, C═N), 1583 (s, C═C), 1468 (m, pz, C═N). ^{1}H NMR (300 MHz, DMSO-d_6, δ (ppm)): 2.32 (s, 3H, pz, −CH_3), 6.56 (s, 1H, pz, –CH), 7.21–8.15 (5 m, 6H, aromatic), 9.65 (s, 1H, –CH═N), 12.04 (s, 1H, −OH), 12.93 (s, 1H, pz, −NH), 13.20 (s, 1H, NNH). ^{13}C NMR (300 MHz, DMSO-d_6, δ (ppm)): 10.70 (pz, −CH_3), 104.98 (pz, −CH), 108.56, 119.45, 120.82, 123.62, 123.87, 127.78, 128.03, 129.63, 132.68, 157.93 (naphthalene moiety), 140.31, 145.26 (pyrazolyl moiety), 147.03 (−CH═N), 157.83 (carbonyl). UV–Vis [DMSO, λ_{max}/nm (ε/M^{-1} cm^{-1})]: 262 (2.53 × 10^4), 300 (7.78 × 10^3), 312 (1.54 × 10^4), 325 (2.28 × 10^4), 345 (1.36 × 10^4), 360 (2.06 × 10^4), 375 (1.91 × 10^4), 435 (4.13 × 10^2).

*2.3.1.6. (E)-N′-((3-hydroxynaphthalen-2-yl) methylene)-5-methyl-1-(pyridine-2-yl)-pyrazole-3-carbohydrazide (**L6**)*. Compound **L6** was prepared by reaction of 5-methyl-1-(2-pyridyl)pyrazole-3-carbohydrazide [16] (434 mg, 2.00 mmol) with 2-hydroxy-1-naphthaldehyde (344 mg, 2.00 mmol). (Yield: 502 mg, 67.5%) ESI-MS (MeOH) *m/z* [Found (Calcd)]: 370.6 (371.14) (51%) [L − H]$^-$. *Anal.* Calc. for $C_{21}H_{17}N_5O_2$: C, 67.91; H, 4.61; N, 18.86. Found: C, 68.0; H, 4.7; N, 18.5%. FTIR (KBr, cm^{-1}): 3423 (br, −N−NH and −OH), 1707 (m, −C═O), 1666 (s, C═N), 1592 (m, C═C), 1473 (m, pz, C═N). ^{1}H NMR (300 MHz, DMSO-d_6, δ (ppm)): 2.71 (s, 3H, pz, −CH_3), 6.85 (s, 1H, pz, −CH), 7.24, 7.42, 7.61, 7.91, 7.94, 8.22 (m, 6H, naphthalene moiety), 7.51, 8.05, 8.12, 8.59 (m, 4H, pyridine substituent), 9.56 (s, 1H, −CH═N), 12.10 (s, 1H, −OH), 12.79 (s, 1H, NNH). ^{13}C NMR (300 MHz, DMSO-d_6, δ (ppm)): 14.15 (pz, −CH_3), 109.68 (pz, −CH), 109.20, 119.15, 120.99, 123.69, 124.49, 128.17, 129.45, 132.70, 132.98, 158.41 (naphthalene moiety), 142.43, 143.28 (pyrazolyl moiety), 147.54 (−CH═N), 153.30 (carbonyl), 117.56, 123.45, 138.80, 139.56, 148.49 (pyridine substituent). UV–Vis [DMF, λ_{max}/nm (ε/M^{-1} cm^{-1})]: 268 (1.66 × 10^4), 275 (1.57 × 10^4), 312 (1.29 × 10^4), 325 (1.91 × 10^4), 346 (1.18 × 10^4), 361 (1.78 × 10^4), 377 (1.64 × 10^4).

2.3.2. Synthesis of the complexes

2.3.2.1. Complex C1 (L1 + $CuCl_2{\cdot}2H_2O$). To a solution of **L1** (289 mg, 0.887 mmol) in methanol (10 mL), $CuCl_2{\cdot}2H_2O$ (170 mg, 0.997 mmol) taken in the same solvent was added drop wise with constant stirring in

the presence of two drops of NaOH 0.5 M. Immediately, the solution turned olive green. Stirring was continued for *ca.* 2 h and a green coloured compound separated out from the reaction mixture. The solid was filtered, washed with cold methanol and dried in vacuum. (Yield: 183 mg, 47%); ESI-MS (H_2O) *m/z* [Found (Calcd)]: 351.2 (351.04) (100%) $[M - Cl]^+$. *Anal.* Calc. for $C_{13}H_{14}ClCuN_5O_3{\cdot}NaCl.2.5H_2O$: C, 31.82; H, 3.90; N, 14.27. Found: C, 31.8; H, 3.3; N, 14.1%. FTIR (KBr, cm^{-1}): 3478 (w, pyr, $-CH_2OH$), 2857 (m, pyr, hydrogen bonding), 1575 (s, C=N), 1544 (s, C=C), 1430 (s, pz, C=N). UV–Vis [MeOH, λ_{max}/nm ($\varepsilon/M^{-1}\,cm^{-1}$)]: 236 ($2.20 \times 10^4$), 317 ($8.02 \times 10^3$), 332 ($9.60 \times 10^3$), 345 ($9.85 \times 10^3$), 383 ($9.16 \times 10^3$), 401 ($1.48 \times 10^4$), 419 ($1.64 \times 10^4$).

2.3.2.2. Complex C2 (L2 + $CuCl_2{\cdot}2H_2O$). To a hot solution of **L2** (122 mg, 0.499 mmol) in methanol (10 mL), $CuCl_2.2H_2O$ (85 mg, 0.499 mmol) taken in H_2O/MeOH (8 mL, 1:2 v/v) was added drop wise with constant stirring at 55 °C in the presence of two drops of NaOH 0.5 M. Immediately, the solution turned olive green and the stirring was continued for *ca.* 5 h. A green coloured compound separated out from the reaction mixture. This was filtered, washed with cold methanol and dried in vacuum. (Yield: 140 mg, 82%); ESI-MS (MeOH) *m/z* [Found (Calcd)]: 337.8 (337.99) (90%) $[M - Cl + MeOH]^+$; 340.4 (339.99) (100%) $[M\text{-}H]^-$. *Anal.* Calc. for $C_{12}H_{11}ClCuN_4O_2$: C, 42.11; H, 3.24; N, 16.37. Found: C, 42.3; H, 3.5; N, 16.2%. FTIR (KBr, cm^{-1}): 1618 (s, azomethine, C=N), 1539 (s, C=C), 1440 (m, pz, C=N). UV–Vis [DMF, λ_{max}/nm ($\varepsilon/M^{-1}\,cm^{-1}$)]: 269 ($1.40 \times 10^4$), 287 ($1.28 \times 10^4$), 298 ($1.41 \times 10^4$), 313 ($1.38 \times 10^4$), 327 ($1.22 \times 10^4$), 383 ($1.02 \times 10^4$), 396 ($1.08 \times 10^4$).

2.3.2.3. Complex C3 (L3 + $CuCl_2{\cdot}2H_2O$). Compound **C3** was synthesized in a procedure similar to the one used for **C1** with **L3** (272 mg, 0.992 mmol) instead of **L1**. A green coloured product was obtained. (Yield: 302 mg, 81%); ESI-MS (MeOH) *m/z* [Found (Calcd)]: 336.2 (336.00) (50%) $[M - Cl]^+$; 273.5 (273.11) $[M - H]^-$ (100%); 370.2 (370.00) (62%) $[M - H]^-$. *Anal.* Calc. for $C_{13}H_{13}ClCuN_4O_3{\cdot}0.3H_2O$: C, 41.34; H, 3.63; N, 14.83. Found: C, 41.5; H, 3.7; N, 14.6%. FTIR (KBr, cm^{-1}): 1617 (s, N=CO), 1605 (s, azomethine, −C=N), 1549 (s, C=C), 1440 (s, pz, C=N). UV–Vis [DMSO, λ_{max}/nm ($\varepsilon/M^{-1}\,cm^{-1}$)]: 261 ($1.48 \times 10^4$), 300 ($1.30 \times 10^4$), 313 ($1.43 \times 10^4$), 325 ($1.41 \times 10^4$), 338 ($1.13 \times 10^4$), 401 ($7.48 \times 10^3$).

2.3.2.4. Complex C4 (L4 + $CuCl_2{\cdot}2H_2O$). Compound **C4** was synthesized in a procedure similar to the one used for **C2** with **L4** (144 mg, 0.499 mmol) instead of **L2**. A green coloured product separated out from the reaction mixture. (Yield: 168 mg, 87%); ESI-MS (MeOH) *m/z* [Found (Calcd)]: 428.05 (428.3) [M + Acetonitrile + H]$^+$ (90%); 384.3 (384.01) (85%) $[M - H]^-$. *Anal.* Calc. for $C_{14}H_{15}ClCuN_4O_3{\cdot}0.7H_2O$: C, 42.15; H, 4.14; N, 14.05. Found: C, 42.3; H, 4.1; N, 13.8%. FTIR (KBr, cm^{-1}): 1619 (s, −N=CO), 1602 (s, azomethine C=N), 1540 (s, C=C), 1442 (s, pz, C=N). UV–Vis [DMSO, λ_{max}/nm ($\varepsilon/M^{-1}\,cm^{-1}$)]: 260 ($1.13 \times 10^4$), 313 ($1.04 \times 10^4$), 326 ($1.10 \times 10^4$), 339 ($9.37 \times 10^3$), 401 ($6.78 \times 10^3$).

2.3.2.5. Complex C5 (L5 + $CuCl_2{\cdot}2H_2O$). Compound **C5** was synthesized in a procedure similar to the one used for **C1** with **L5** (294 mg, 0.999 mmol) instead of **L1**. A green coloured product separated out from the reaction mixture. (Yield: 301 mg, 76.8%); ESI-MS (MeOH) *m/z* [Found (Calcd)]: 455.1 (455.03) [M + Acetonitrile + Na]$^+$ (100%). *Anal.* Calc. for $C_{16}H_{13}ClCuN_4O_2.1.1H_2O$: C, 46.63; H, 3.72; N, 13.59. Found: C, 46.6; H, 3.4; N, 13.1%. FTIR (KBr, cm^{-1}): 3235 (m, NH), 1634 (m, −C=O), 1575 (m, azomethine, C=N), 1546 (s, C=C), 1456 (m, pz, C=N). UV–Vis [DMSO, λ_{max}/nm ($\varepsilon/M^{-1}\,cm^{-1}$)]: 262 ($2.41 \times 10^4$), 271 ($2.39 \times 10^4$), 310 ($9.15 \times 10^3$), 325 ($1.16 \times 10^4$), 333 ($1.15 \times 10^4$), 382 ($6.81 \times 10^3$), 415 ($1.24 \times 10^4$), 433 ($1.23 \times 10^4$).

2.3.2.6. Complex C6 (L6 + $CuCl_2{\cdot}2H_2O$). Compound **C6** was synthesized in a procedure similar to the one used for **C2** with **L6** (110 mg, 0.296 mmol) instead of **L2**. A green coloured product separated out from the reaction mixture, after *ca.* 5 h. (Yield: 116 mg, 85.5%); ESI-MS (MeOH) *m/z* [Found (Calcd)]: 433.4 (433.94) $[M - Cl]^+$ (100%). *Anal.* Calc. for $C_{21}H_{16}ClCuN_5O_2{\cdot}2H_2O$: C, 49.91; H, 3.99; N, 13.86. Found: C, 49.8; H, 3.3; N, 13.6%. FTIR (KBr, cm^{-1}): 3434 (br, −N−NH), 1664 (s, −C=O), 1612 (s, C=N), 1600 (m, C=C), 1460 (s, pz, C=N). UV–Vis [DMF, λ_{max}/nm ($\varepsilon/M^{-1}\,cm^{-1}$)]: 268 ($2.19 \times 10^4$), 283 ($2.69 \times 10^4$), 326 ($1.33 \times 10^4$), 340 ($1.63 \times 10^4$), 395 ($1.15 \times 10^4$), 416 ($1.81 \times 10^4$), 435 ($1.54 \times 10^4$).

2.3.3. Chloride analysis by ion exchange chromatography

Solutions of **C1** in water and **C3** and **C5** in DMSO (*ca.* 4 mM) were hydrolysed with a solution 0.1 M of H_2SO_4 by stirring overnight at room temperature. The resulting solutions were diluted with Millipore water so that the expected Cl^- concentration was within the range of the measured calibration curve. A calibration curve was obtained with five solutions of KCl, prepared from a 500 ppm stock solution in Millipore water, with concentrations ranging from 2.0 to 25 ppm. The diluted, hydrolysed solutions of the complexes were injected into the chromatographic system and the chloride concentration determined.

2.3.4. X-ray crystal structure determination

Three-dimensional X-ray data were collected on a Bruker Kappa Apex CCD diffractometer at low temperature for **L2** and **L3**, by the ϕ-ω scan method. Reflections were measured from a hemisphere of data collected from frames, each of them covering 0.3° in ω. A total of 66,637 for **L2** and 13,277 for **L3** reflections measured were corrected for Lorentz and polarization effects and for absorption by multi-scan methods based on symmetry-equivalent and repeated reflections. Of the total, 3399 for **L2** and 2459 for **L3** independent reflections exceeded the significance level ($|F|/\sigma|F|$) > 4.0, respectively. After data collection, in each case, an empirical absorption correction (SADABS) [17] was applied, and the structures were solved by direct methods and refined by full matrix least-squares on F^2 data using SHELX suite of programs [18–20]. In **L2**, hydrogen atoms were located in difference Fourier map and left to refine freely, except for C(5) and C(17), which were included in calculated positions and refined in the riding mode. In **L3**, hydrogen atoms were located in difference Fourier map and left to refine freely, except for C(5) and C(13), which were included in calculated positions and refined in the riding mode. Refinements were done with allowance for thermal anisotropy of all non-hydrogen atoms. A final difference Fourier map showed no residual density outside: 0.414 and − 0.323 e·Å^{-3} for **L2** and 0.168 and − 0.128 e·Å^{-3} for **L3**. A weighting scheme $w = 1 / [\sigma^2(F_o^2) + (0.085900P)^2 + 0.00000P]$ for **L2** and $w = 1 / [\sigma^2(F_o^2) + (0.034600P)^2 + 0.327200P]$ for **L3**, where $P = (|F_o|^2 + 2|F_c|^2) / 3$, were used in the latter stages of refinement. Further details of the crystal structure determination are given in Table 1. CCDC 1532353–1532354 contain the supplementary crystallographic data for the structures reported in this paper. These data can be obtained free of charge *via* http://www.ccdc.cam.ac.uk/conts/retrieving.html, or from the Cambridge Crystallographic Data Centre, 12 Union Road, Cambridge CB2 1EZ, UK; fax: (+ 44) 1223 336 033; or e-mail: deposit@ccdc.cam.ac.uk.

2.3.5. Stability studies in aqueous medium

Stock solutions of the complexes were prepared in DMSO (except complex **C1** which was dissolved in water) with a concentration of 500 μM. Dilutions were then prepared containing 125 μL of the stock solution and 2375 μL of PBS buffer (pH 7.4, 10 mM), having a final complex concentration of 25 μM and 5% DMSO. The UV–Visible spectra (250–700 nm) were recorded for 2½ h, with 5 min between each two consecutive measurements. Two other spectra were recorded after 3 and 24 h.

Table 1
Crystal data and structure refinement for **L2** and **L3**.

	L2	L3
Formula	$C_{12}H_{12}N_4O_2$	$C_{13}H_{14}N_4O_3$
Formula weight	244.26	274.28
T, K	100(2)	100(2)
Wavelength, Å	0.71073	0.71073
Crystal system	Monoclinic	Monoclinic
Space group	$P2_1/c$	Cc
a/Å	25.1099(8)	10.9504(4)
b/Å	7.4673(3)	10.3636(3)
c/Å	12.5831(4)	11.4465(3)
β/°	98.503(2)	98.9312(18)
V/Å^3	2333.44(14)	1283.26(7)
Z	8	4
F_{000}	1024	576
D_{calc}/g cm^{-3}	1.391	1.420
μ/mm^{-1}	0.099	0.104
θ/(°)	0.82 to 26.44	3.10 to 26.38
R_{int}	0.0637	0.0259
Crystal size/mm^3	0.43 × 0.12 × 0.12	0.28 × 0.12 × 0.12
Flack parameter (x)		0.0(8)
Goodness-of-fit on F^2	1.062	1.046
$R_1[I > 2\sigma(I)]$[a]	0.0444	0.0279
wR_2 (all data)[b]	0.1382	0.0661
Largest differences peak and hole (e·Å^{-3})	0.414 and −0.323	0.168 and −0.128

[a] $R_1 = \Sigma||F_o| - |F_c|| / \Sigma|F_o|$.
[b] $wR_2 = \{\Sigma[w(|F_o|^2 - |F_c|^2|)^2]| / \Sigma[w(F_o^2)^2]\}^{1/2}$.

2.3.6. Evaluation of the antioxidant activity

The compounds were dissolved in DMSO at an initial concentration of 1 mM. A 98.5 μM solution of DPPH (1,1-diphenyl-2-picryl-hydrazyl) in methanol (2 mg/50 mL) was prepared as stock, and kept in the dark during the entire assay. Five samples were prepared with a final volume of 2500 μL, containing 1500 μL of DPPH and different volumes of the compounds' solution and methanol, in order to obtain molar ratios n (compound)/n(DPPH) of 0, 25, 50, 75 and 100%. These were vigorously shaken and kept in the dark for 30 min. The absorbance was recorded between 300 and 700 nm. The antioxidant activity (% scavenging activity) is calculated as.

$$\%ScavAct = \left(\frac{A_0 - A_f}{A_0}\right)100 \quad (1)$$

where A_0 and A_f are the absorbance values at 516 nm in the absence and presence of the compound, respectively. The IC_{50} value (the concentration required to scavenge DPPH radical by 50%) is determined by a linear regression where the % of scavenging activity is 50. The procedure was also done for a known antioxidant: ascorbic acid, the positive control (PC).

2.4. Biological assays

2.4.1. Preparation of solutions for biological assays

Stock solutions of DNA were prepared by dissolving the nucleic acid in PBS buffer (pH 7.4), kept at 4 °C for about 48 h and used within a week. Solutions of DNA gave ratios of absorbance A_{260}/A_{280} of *ca.* 1.9, indicating that the DNA was sufficiently protein free [21,22]. The concentration of the prepared *ct*DNA stock solutions were calculated based on their absorbance at 260 nm by using the per nucleotide extinction coefficient $\varepsilon_{260} = 6600\ M^{-1}\ cm^{-1}$ [22].

The thiazole orange (TO) solution was prepared by dissolving ~1 mg of the compound in 6 mL of deionized water, providing a solution with 317 μM concentration, which was used in the same day.

The fatty acid free HSA solutions were prepared by dissolving the protein in PBS buffer (pH 7.4). The solutions were gently swirled and allowed to equilibrate overnight at 4 °C. They were used within 24 h. The HSA concentrations were estimated spectrophotometrically considering an extinction coefficient of 36,850 $M^{-1}\ cm^{-1}$ at 280 nm [23]. Typically, the concentration of the HSA stock solution was *ca.* 40 μM.

2.4.2. Thiazole orange displacement assays

Prior to titration with the complexes, DNA was saturated with thiazole orange. Selected volumes of the *ct*DNA and TO stock solutions were added in the fluorescence cuvette, with a total volume of 2500 μL completed with PBS buffer, in order to ensure a molar ratio TO/DNA of 0.8. The fluorescence emission spectrum was recorded between 520 nm and 700 nm. The following parameters were used: λ_{exc} = 509 nm, excitation and emission bandwidths of 5 nm.

Successive aliquots of the complexes' stock solutions were added directly to the cuvette and the fluorescence emission spectra were recorded for each of them. Blank assays were done for each complex where the fluorescence under the same concentrations for *ct*DNA and complex was recorded and subtracted from each corresponding emission spectrum.

The decrease of the fluorescence emission intensity at 530 nm, the emission maximum, was analyzed according to the Stern-Volmer equation to determine the fluorescence quenching constant:

$$I_0/I = 1 + K_{SV}[Q] \quad (2)$$

where I_0 and I are the fluorescence emission intensities of the TO-*ct*DNA solutions in the absence and in the presence of quencher, respectively, K_{SV} is the linear Stern-Volmer quenching constant, dependent on the ratio between the bound concentration of TO and the concentration of DNA, and [Q] is the molar concentration of the quencher. A plot of I_0/I *versus* [Q] will give K_{SV} as the slope.

2.4.3. DNA cleavage activity

The plasmid DNA (pDNA) used for gel electrophoresis experiments was pA1, which consists of a full-length cDNA from Cytochrome P4baby50 CYP3A1 inserted in the PBS plasmid vector (pBluescribe, Strata-gene, UK) and described elsewhere [24]. See Supplementary information for further details.

2.4.4. HSA binding studies

To evaluate the interaction of the complexes with HSA, to a solution of *ca.* 1.5 μM of HSA in PBS (pH 7.4), successive aliquots of a stock solution of each complex in DMSO were added directly to the cuvette (optical path 1.0 cm) and the fluorescence emission was recorded between 305 and 700 nm with excitation at 295 nm, and excitation and emission bandwidths of 5 nm. The DMSO % was kept below 2%. The maximum emission wavelength is close to the Raman peak upon excitation at 295 nm. Therefore, for the Stern-Volmer plots, the emission at 340 nm was used and blank samples (in the absence of HSA) with the same concentration of the complexes were recorded and subsequently subtracted from the corresponding emission spectra containing the fluorophore. Moreover, the fluorescence emission intensity was corrected for the absorption and inner filter effects using UV–Visible absorption data recorded for each sample, since all complexes show absorption in the measured region [25,26].

2.4.5. Cell viability assays

The tumour cell lines MCF7 (breast) and PC3 (prostate) were cultured in DMEM (Dulbecco's Modified Eagle Medium) containing GlutaMax I (MCF7) and RPMI 1640 (PC3) culture medium (Invitrogen) supplemented with 10% FBS and 1% penicillin/streptomycin at 37 °C in a humidified atmosphere of 5% CO_2 (Heraeus, Germany). Cell viability was evaluated using a colorimetric method based on the tetrazolium salt MTT (MTT = [3-(4,5-dimethylthiazol-2-yl)-2,5-diphenyltetrazolium bromide]), which is reduced in viable cells to yield purple formazan crystals. Cells were seeded in 96-well plates at a density of 2×10^4 cells (PC3) and 5×10^4 cells (MCF7) per well in 200 μL of culture medium and left to incubate overnight for optimal adherence.

After removal of the medium, 200 µL of a dilution series of the compounds (from stock solutions of 10 or 5 mM in DMSO) in fresh medium were added and incubation was performed at 37 °C/5% CO_2 for 48 h. For the higher concentrations controls of 1% DMSO were done. At this concentration DMSO did not present cytotoxic effects. At the end of the incubation period, the compounds were removed and 200 µL of a MTT solution (500 µg/mL) was added to the cells. After further incubation for 3 h at 37 °C/5% CO_2, the medium was removed and the purple formazan crystals were dissolved in 200 µL of DMSO by shaking. The cell viability was evaluated by measurement of the absorbance at 570 nm using a plate spectrophotometer (Power Wave Xs, Bio-Tek). The cell viability was calculated dividing the absorbance of each well by that of the control wells (untreated cells) and expressed as a percentage. Each experiment was repeated at least twice and each concentration was determined in at least six replicates.

2.4.6. Apoptosis assays

The effect of selected complexes on caspases 3/7 was determined in the prostate cancer cells PC3 using the Caspase-Glo® 3/7 Assay (Promega). Briefly, cells, plated in 96 wells were treated with complexes **C5** and **C6** for 48 h at concentrations equivalent to their IC_{50} values. After 48 h, the medium was removed from each well and the caspase reagent was added in a 1:1 (v/v) in medium and the plate was shaken in an orbital shaker for 30 s at 300–500 rpm. The plate was incubated at room temperature and the luminescence was measured using an Infinite 200 Plate Reader (Tecan). Each experiment was repeated twice and each concentration was tested with at least three replicates. Results (mean ± SD) were expressed as RLU (relative luminescent units).

2.4.7. Imaging Cu distribution in cells

PC3 cells (3–6 × 10^5) were prepared for nuclear microscopy experiments by seeding the cells on silicon frames with 5 × 3 windows of 0.56 mm^2 covered with 100 nm thick silicon nitride membrane (Silson Ltd., UK), in 6-well plates and incubated overnight. The silicon nitride windows were previously sterilized with UV light. Cells were incubated with complex **C6** for 24 h at 20 µM (IC_{50} at 24 h) and 2 h at 200 µM at 37 °C in a 5% CO_2 incubator. After incubation the medium was removed and the windows were washed with cold PBS. Samples were frozen at − 80 °C and then dried in a cryostat at − 25 °C for subsequent analysis.

The elemental distributions were carried out using the nuclear microscopy facility of the CTN/IST [27]. A 2.0 MeV proton beam was focused down to of 2 μm^2 and scanned across the target cell on the silicon nitride window. The simultaneous application of PIXE (Particle Induced X-ray Emission), RBS (Rutherford Backscattering Spectroscopy) and STIM (Scanning Transmission Ion Microscopy) deliver images of the sample morphology besides providing information on the elemental distributions of and concentrations. By scanning whole cells, images of the chemical elemental distributions, such as Cu and other physiologically relevant elements in individual cells can be produced. Point analyses in selected transepts across cells rendering concentration profiles were produced. Spectral and positional information were recorded using the OMDAQ [28] acquisition system and elemental concentrations were calculated with the Dan32 program as described elsewhere [29,30]. Images of whole PC3 cells were taken with 25 × 25 μm^2 scan sizes.

3. Results and discussion

3.1. Synthesis and characterization of ligands

The Schiff bases derived from pyrazole were synthesized by condensation of the corresponding carbohydrazide with different aldehydes (see Scheme 1). The reactions were carried out in methanol with a catalytic amount of acetic acid to ensure the formation of the azomethine and separation of the product from the mixture. Moderate to good yields (60–88%) were obtained. They were characterized by elemental analysis, spectroscopic techniques and single crystal X-ray diffraction — see Experimental part and Table S1 in Supplementary Information.

^{1}H NMR spectroscopy confirms the presence of the azomethine proton (**H**C═N) [31] — see Table S1. Another peak that was clearly identified at δ 2.30 ppm, integrating for 3 protons, was unambiguously assigned to the methyl group attached to the pyrazole ring. Moreover, the effect of having a pyridine ring as substituent in the nitrogen can be observed since this signal appears at 2.32 ppm for **L5** and at 2.71 ppm for **L6** [16]. FTIR spectroscopy allowed the identification of characteristic functional groups [16,32–34]. The band corresponding to the stretching vibration of the azomethine ν(C═N) appears between 1592 cm^{-1} and 1626 cm^{-1}, as expected for a Schiff base coupled to an aromatic ring [35]. The frequency for the C−O stretching in the phenol group appears at lower wavenumbers [36].

The UV–visible electronic absorption spectra of the ligands were recorded in MeOH for **L1**, DMF for **L2** and **L6**, and DMSO for **L3**–**L5**, according to the solubilities of the corresponding complexes, since all ligands are soluble in any of these solvents. The spectra of all Schiff bases present two set of bands corresponding to n → π* (325 nm to 377 nm) and π → π* (276 nm to 325 nm) transitions of both the carbonyl moiety and imine bonds, present in the molecules [37–39]. Moreover, for compounds **L5** and **L6**, sharing a naphthalene moiety, it was also possible to assign the bands corresponding to the π → π* (262 nm to 275 nm) transition of the aromatic rings. Compounds **L1**–**L6** were also characterized by electrospray ionization mass spectrometry (ESI-MS) and the peaks corresponding to the molecular ion were identified in the positive and/or negative mode, according to the calculated exact mass [32]. The assignments are listed in Table S1. Other peaks corresponding to species $[L + Na]^+$, $[L + Cl]^-$, $[2L + H]^+$ and $[2L - H]^-$ were also identified (see experimental section).

The molecular structure of **L1**–**L6** was further confirmed by the crystal structure obtained for **L2** and **L3** by single crystal X-ray diffraction — see the ORTEP diagrams of **L2** and **L3** in Fig. 1. Both molecules crystallize in the monoclinic crystal system (for details see Table 1). Selected bond distances (Å) and angles (°) are listed in Table S2. The asymmetric unit of **L2** contains two molecules, which interact through π-π clouds (see Fig. 1). The distances between π clouds of the centroids between phenyl rings and C═N groups are: d_{c1-c2} = 3.333(5) Å [c1: C(6)-N(2) and c2: C(19)-C(20)-C(21)-C(22)-C(23)-C(24)] and d_{c3-c4} = 3.408(6) Å [c3: C(13)-N(5) and c4: C(2)-C(3)-C(4)-N(3)-N(4)]. The asymmetric unit of **L3** contains only one molecule. The phenyl ring [C(7)-C(8)-C(9)-C(10)-C(11)-C(12)] is almost flat with respect to the pyrazol ring [C(2)-C(3)-C(4)-N(3)-N(4)], the torsion angle being

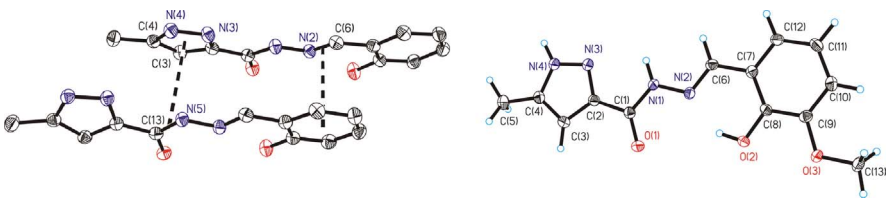

L2 **L3**

Fig. 1. ORTEP plot of compound **L2** and **L3**. The asymmetric unit of **L2** contains two molecules and the π–π stacking interactions in the asymmetric unit of the compound **L2** are shown. All the non-hydrogen atoms are presented by their 50% probability ellipsoids.

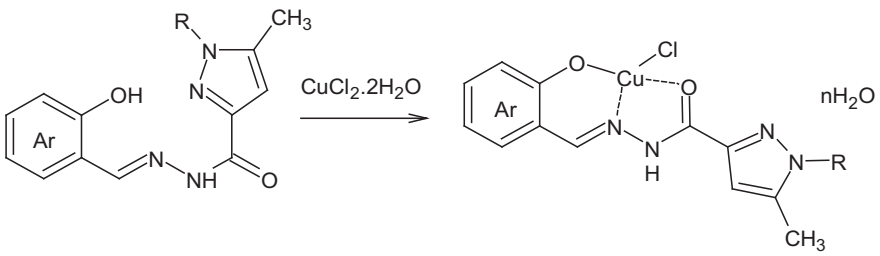

Scheme 2. General synthetic scheme for the formation of the Cu (II)-complexes. R is H or pyridyl and Ar stands for 1 or 2 fused aromatic rings.

7.44(12)°. π–π interactions and hydrogen bonds between the molecules, both in **L2** and **L3** determine the crystal packing (see SI).

3.2. Synthesis and characterization of the complexes

The synthesized compounds **L1–L6** were coordinated to copper(II) by stirring a methanolic solution of both reactants, compounds **L1–L6** and $CuCl_2{\cdot}2H_2O$, for a few hours at *ca.* 50 °C, in the presence of NaOH (0.5 M) — see Scheme 2. In all syntheses a green compound separated from the reaction mixture (**C1–C6**) in moderate to good yields (47–87%).

Upon coordination of the ligands to copper(II) changes are expected in their spectroscopic signatures. In the FTIR spectra the deprotonation and coordination of the phenolic oxygen leads to the disappearance of its OH stretching band - see SI. It should be noted that the free ligands have two keto-enol tautomers, in which the proton can be found in the N- or the O-atoms. However, all data supports coordination in the keto form. Since upon coordination the NH bond cannot stretch with the same intensity as in the free ligand, this band is included in a broad envelope centered around 3300–3400 cm^{-1} due to the presence of water molecules in the structure. As expected, the bands corresponding to the carbonyl (C═O) and to the azomethine (C═N) shift to lower wavenumbers upon coordination to the copper center [34,40].

Characterization of the complexes by UV–Vis electronic absorption spectroscopy is included in SI and in Fig. 2. Complex **C1** is very soluble in water and sparingly in DMSO (1 mM). All other complexes are soluble in DMSO (3 mM) after 1 h under sonication. Overall, bands ranging from 280 nm to 460 nm in all the complexes' spectra have similar origin as the bands from the corresponding ligands, ranging from 260 nm to 400 nm, arising mainly from transitions within the imine and carbonyl moieties. Additionally, the strong band(s) appearing at *ca.* 430–440 nm for complexes **C1–C6** are due to charge transfer transitions between metal and ligand [38,41]. Bands for the $\pi \rightarrow \pi^*$ transition of the naphthalene moiety of **C5** and **C6** (at *ca.* 270 nm) do not suffer much changes when compared to the respective ligands, since this part of the molecule is not directly involved in the coordination to the metal ion. As expected for Cu(II) complexes with a d^9 configuration, d–d transitions appear as broad bands centered around 700 nm in DMSO [37,42].

All complexes were also characterized by electron paramagnetic resonance (EPR). The spectra were measured in DMSO (and methanol for **C1**) at 77 K — see Fig. 3 and SI section. The spin Hamiltonian parameters were obtained by computer simulation of the experimental spectra using a program from Rockenbauer and Korecz [43] and are presented in Table 2.

Due to i) poor solubility of the complexes, ii) high viscosity of the DMSO solutions, and iii) high dielectric constant of DMSO, spectra with poor resolution and broad bands were obtained in most cases. Moreover, superhyperfine splitting due to coupling of the electron spin with the ^{14}N nucleus ($I = 1$) was not observed, but this is often the case under these measurement conditions. All complexes, except **C2**, originate axial spectra. For this compound, only one broad signal at $g \sim 2.1$ (see SI section) is observed, suggesting the presence of extensive exchange coupling between the molecules [44]. For all other complexes $g_z > g_{x,y} > 2.0$, indicating the presence of a $d_{x^2-y^2}$ ground state in copper(II), located in square-based geometries.

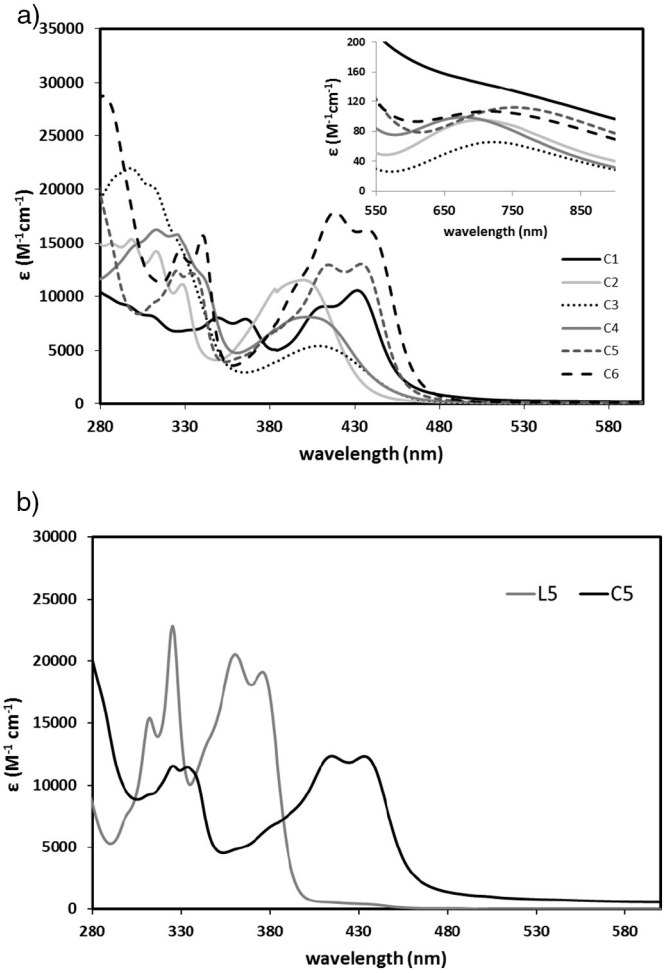

Fig. 2. UV–visible electronic absorption spectra of a) 0.1 mM solutions of the complexes in DMSO; *Inset*: Spectra measured in the visible range for 3 mM solutions (DMSO) showing the d-d band (after 1 h of sonication). b) UV–visible electronic absorption spectra of **L5** and **C5** in (0.1 mM) DMSO solution.

The Peisach-Blumberg plot [45], updated by Sakagushi and Addison [46] correlates A_z with g_z and introduces the empirical parameter, known as the tetrahedral distortion index, g_z/A_z. The plot of A_z *vs.* g_z, included in SI section, shows that the parameters for complexes **C1–C6** fall in the region usually found for N_4, N_2O_2 and O_4 coordination. Moreover, since for **C1–C5**, g_z/A_z = 119–134 ($\times 10^4$ cm), then, square planar geometries can be assigned to these complexes, while in **C6** strong tetrahedral distortions must be present [46].

The complexes were also characterized by ESI-MS (see SI) and the assignment is presented in Table 3. It was always possible to make relevant assignments. Moreover, in all assigned complexes' peaks, the isotopic pattern due to ^{63}Cu and ^{65}Cu was observed.

Combining all the analytical data on the complexes, namely elemental analysis and spectroscopic studies, binding modes involving the

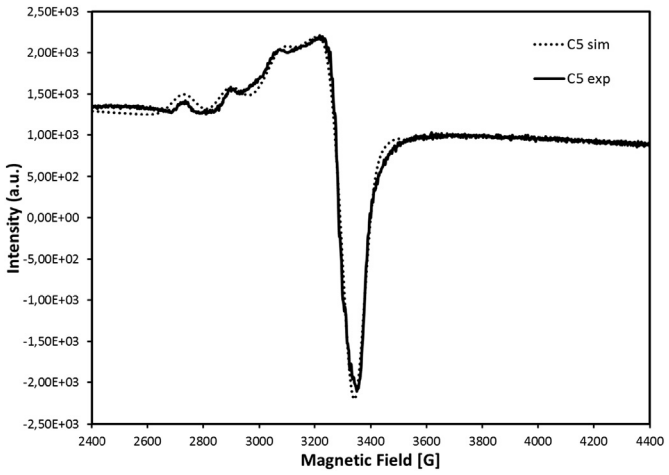

Fig. 3. First derivative X-band EPR spectra of complex **C5**, 1 mM in DMSO, measured at t = 77 K. The experimental spectra are presented in red and the simulated in blue (see Table 2 for parameters). (For interpretation of the references to colour in this figure legend, the reader is referred to the web version of this article.)

ligand coordinated in a keto form, through O-phenolate, N-imine and O-carbonyl atoms, are proposed. The coordination sphere and neutrality of the Cu(II)-complexes is achieved through additional coordination of a chloride ion. The presence of the chloride ions (either coordinated or as counter ions) is suggested by the CNH elemental analysis and confirmed by ion exchange chromatography. Data (not shown) showed that two chloride ions are present in the structure of **C1**, while only one was detected in each of the complexes' structures of **C3** and **C5** (Cl^- was not analyzed in the other complexes). Therefore we can conclude that in **C1** there is probably a salt (NaCl) molecule trapped in the structure — see Scheme 3.

3.3. Stability studies

Since biological studies are carried out in aqueous media at physiological pH it is necessary to ensure that the complexes do not precipitate in the aqueous environment and that they are stable in the timescale of the studies. Thus, the stability of the complexes was evaluated by UV–Vis spectroscopy in buffered solutions of pH 7.4 containing a minimum amount of organic solvent, needed to solubilize the metal complexes. Changes observed with time for each complex solution were followed through UV–Visible spectroscopy. Only **C4** and **C5** showed some degradation during the time frame of the study (24 h), as depicted in Supplementary Information. **C2**, **C3** and **C6** showed some solubility issues, precipitating after a few hours and therefore lower absorbance values were recorded with time. However, in the first 3 h only small changes occurred. Complex **C1** maintains its original form in solution, even after a long period of time. Most of the observed changes are due to the low solubility of the complexes in the aqueous media and therefore since lower concentrations are used in the biological assays we expect that both the stability and the solubility are not compromised.

3.4. Radical scavenging activity

The antioxidant activity of the compounds was evaluated, as it is an important property for the detoxification of free radicals that are formed in the oxygen metabolism. Schiff base ligands and metal complexes have been studied as antioxidant agents against free radicals [10]. Scavenging of the DPPH free radical is the basis of a common antioxidant assay [47]. The antioxidant activity of all compounds was determined as well as the IC_{50}, the concentration required to scavenge 50% of the DPPH activity, the results being presented in Table 4.

None of the tested compounds shows significant antioxidant activity as can be seen from the values included in Table 4. When compared with the positive control, ascorbic acid, the IC_{50} values of the tested compounds are substantially higher, implying that most of them do not behave as antioxidants. In some cases, the copper complexes showed better activity than the corresponding ligands, as in the case of **C2**, **C3** and **C5**. On the contrary, in **C1** and **C4** the presence of Cu(II) has a negative effect in the antioxidant power, with **C1** showing a higher IC_{50} value when compared with **L1**, which is the best among **L1–L5**; and **C4** having no activity. Overall, it can be concluded that the best compound is **L1** (IC_{50} = 49.6 μM), which is the ligand derived from pyridoxal.

When **L6** was tested no activity was recorded while with **C6** an increase in the absorbance was obtained, meaning that the concentration of radicals in solution was increased – see SI.

3.5. Interaction with biological molecules

3.5.1. Interaction with ctDNA

In order to investigate if the complexes are able to interact with DNA, a competition fluorescence quenching study with thiazole orange (TO), a known DNA intercalator, and *calf thymus* DNA (*ct*DNA) was done for some complexes. Interactions with DNA are of extreme importance when evaluating compounds for anti-cancer applications. Since cancer is characterized by a highly genomic instability [2], the genetic material is a preferential target for anti-cancer drugs. The fact that the mechanism of action of *cisplatin* involves DNA binding is another reason to evaluate this property.

Fluorescence spectroscopy is a simple method to examine the DNA binding mode of metal complexes, and competitive binding experiments based on the displacement of the intercalating probe TO from *ct*DNA can give valuable information. If the complex displaces TO from DNA, the fluorescence of TO decreases due to free molecules being less fluorescent than the DNA bound molecules, since TO becomes more accessible to quenching by solvent molecules. However, not only the DNA intercalators but also DNA groove binders can cause the reduction in the emission intensity of DNA bound TO, but to a lower extent [48].

Fig. 4 shows the emission spectra obtained upon addition of compound **C5** to solutions containing molar ratios of TO:DNA = 0.8. Similar studies were conducted with complexes **C3–C6** and the quenching % upon their addition is depicted in Fig. 4B.

With the exception of **C3**, all tested complexes (**C4–C6**) were able to reduce the fluorescence intensity (to 69–22%), indicating that they are able to compete with TO for the same binding sites, or interact with DNA at different sites, near the bound TO. Since complexes **C1** and **C2** have structures similar to **C3** and **C4**, and these did not show significant

Table 2
Spin Hamiltonian parameters for the Cu(II)-complexes obtained by computer simulation of the experimental spectra [43].

Complex	$g_{x,y}$	g_z	$A_{x,y}$ ($\times 10^{-4}$ cm^{-1})	A_z ($\times 10^{-4}$ cm^{-1})	g_z/A_z ($\times 10^4$ cm)
C1	2.069	2.305	0.7	172.2	134
C3	2.083	2.280	1.5	190.3	120
C4	2.079	2.283	1.5	192.2	119
C5	2.081	2.288	5.8	174.1	131
C6	2.062	2.291	0.8	158.1	145

Table 3
Peak assignment for the copper complexes by ESI-MS.

	C1	C2	C3	C4	C5	C6
Peak assignment	$[M-Cl]^+$	$[M-H]^-$	$[M-H]^-$	$[M-H]^-$	$[M + ACN + Na]^+$	$[M-Cl]^+$
Calc. exact mass (g/mol)	351.04	339.99	370.00	384.01	455.03	433.94
Found *m/z*	351.22	340.40	370.22	384.31	455.08	433.42

ACN = acetonitrile.

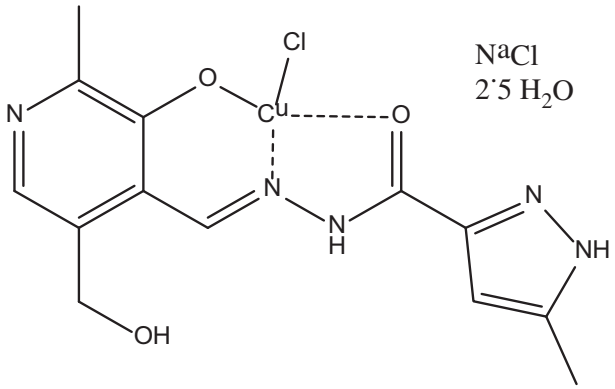

Scheme 3. Proposed structure for complex **C1**.

DNA binding ability, **C1** and **C2** were not tested in this assay.

The quenching data was analyzed through the Stern-Volmer plots (see SI). Generally, the linearity of the Stern-Volmer plot implies the existence of one type of binding site in the proximity of the fluorophore, or several sites equally accessible. Thus, the deviation from linearity of the Stern-Volmer plot indicates the existence of more than one binding site with different accessibilities and/or the occurrence of combined quenching [49].

The apparent binding constant of TO to *ct*DNA has been determined, $K_{TO\text{-}ctDNA} = 3.16 \times 10^5\ M^{-1}$ [50]; and the concentration ratio where the fluorescence intensity is 50% quenched ([Q]) can be obtained from the experimental data, thus, the apparent binding constant for the complex to DNA (K_{app}) can be estimated through:

$$K_{TO-ctDNA}\,[TO] = K_{app}\,[Q] \quad (3)$$

The calculations were done and the results are presented in Table 5. In Supplementary Information details for the evaluation of complexes **C3**–**C6** are given.

Although **C3** and **C4** are structurally similar, the only difference being the length of the substituent on the phenolate ring (methoxy or ethoxy), **C3** is unable to displace TO from DNA, the fluorescence intensity remaining almost unaltered with increasing concentrations of the complex, see Figs. 4B and S16(a) — while **C4** shows quenching ability. Since **C5** and **C6** have larger delocalized π systems, due to the presence of the naphthalene aromatic group, which allows extra van der Waals interactions, they were evaluated following the same procedure. **C1** and **C2** were not tested.

From the analysis of the data included in Table 5 it can be concluded that **C5** is a better TO competitor than any of the other complexes since higher K_{SV} and K_{app} values were obtained. Additional evidence is obtained from the upward curvature towards the *y* axis found in the Stern-Volmer plot of **C5** (see Fig. 5A). This behaviour indicates that the quenching process involves a mixed mechanism. Since a similar result is not obtained with **C6**, possibly because the pyridine substituent at the pyrazole ring imposes larger steric hindrance, it implies that intercalation of the naphthalene ligand is not the only binding mode responsible for the interaction; otherwise, roughly the same K_{SV} values should have been obtained.

In general, a variety of processes can result in fluorescence quenching, usually divided in static and dynamic (energy transfer). Static quenching involves the formation of a ground state complex, but since the emission being monitored is from TO, it can be assumed that static quenching is not driven from the formation of a complex between DNA and the complex, but rather from an influence that **C5** may have by becoming closer to the system — sphere of action [49]. A factor, exp (*V*[**C5**]) where *V* is the static constant and [**C5**] is the total concentration of the complex, can be introduced into the Stern-Volmer equation in order to describe mixed quenching [51].

$$\frac{I_0}{I} = (1 + K_D[\mathbf{C5}])e^{V[\mathbf{C5}]} \quad (4)$$

The static, *V*, and the dynamic, K_D, quenching constants can be obtained by plotting $[I_0/(Ie^{V[C5]})] - 1$ *vs.* [**C5**] till a linear plot is obtained.

The values of K_D and *V* found for **C5** are $(1.05 \pm 0.07) \times 10^5\ M^{-1}$ and $(7.46 \pm 0.04) \times 10^3\ M^{-1}$, respectively. It can be seen that the magnitude of the static quenching constant (*V*) is more than one order of magnitude smaller than the dynamic quenching constant. Overall, it is clear that complex **C5** shows very good ability for interacting with the system TO-*ct*DNA, quenching its fluorescence.

We can therefore conclude that the interaction probably involves π–π stacking between the aromatic rings and the DNA base pairs.

DNA cleavage activity studies were also done but with the exception of **C1**, none of the tested compounds **L2**–**L5** or complexes **C2**–**C5** showed any relevant nuclease activity in the whole concentration range measured (2.5–200 μM), either in the absence or presence of MPA (see Supplemental Information).

3.5.2. HSA binding studies

In order to reach DNA, or any other cellular target, drug needs to reach the cell. Human serum albumin (HSA) plays a key role in mammal organisms, since it is the main transporter of endogenous and exogenous molecules and therefore the determination of a potential drug binding affinity to this protein is crucial. Ceruloplasmin is the major copper-carrying protein in the blood; it carries > 95% of the total copper in healthy human plasma [52]. However, despite the need for copper in ceruloplasmin function, namely its role in iron metabolism, this protein apparently plays no essential role in the transport or metabolism of copper [52] and most studies consider serum albumin as

Table 4
IC_{50} values and molar ratio of compound to DPPH obtained from the DPPH assays for the synthesized compounds.

	L1	C1	L2	C2	L3	C3	L4	C4	L5	C5	L6	C6	AC
IC_{50} (μM)	49.6	364	212	89.2	149	107	156	n.a.	n.a.	66.4	n.a.	n.a	10.9
n(comp)/n(DPPH)	0.84	2.55	3.59	1.56	2.52	1.88	2.65	n.a.	n.a.	1.16	n.a.	n.a.	0.18

n.a. means that no activity was recorded; AC means ascorbic acid (the positive control).

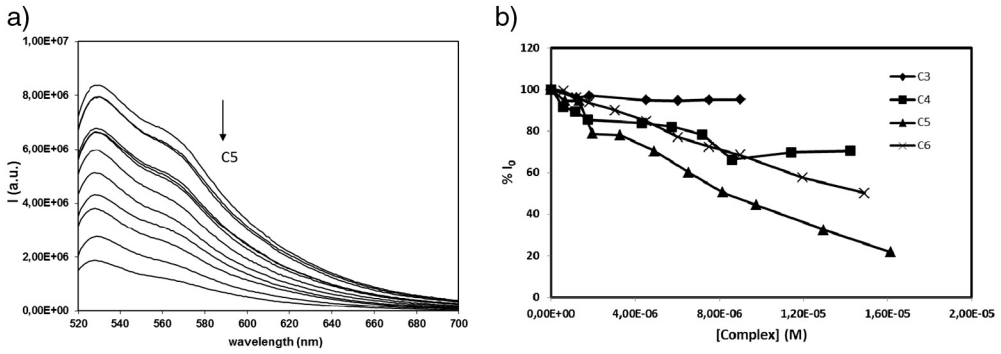

Fig. 4. a) Emission spectra (λ_{ex} = 509 nm) of TO-*ct*DNA (1.6 μM:2.1 μM) in the absence and presence of increasing concentrations of **C5** (0.7–16 μM) in 2% DMSO/PBS pH 7.4, after subtraction of blank emission spectra (arrow indicates variation with increasing concentration of the complex). b) Effect of complexes **C3–C6** in TO-*ct*DNA fluorescence emission: relative fluorescence intensity (%) at emission maxima with increasing complex concentration.

Table 5
Thiazole orange (TO) quenching assay results for Cu-complexes **C3–C6**.

	$K_{SV} \times 10^4$ [M^{-1}]	R^2	Concentration at 50% quenching/μM	$K_{app} \times 10^4$ [M^{-1}]
C3	n.a.	n.a.	n.a.	n.a.
C4	4.8 ± 0.8	0.870	16	3.20
C5	12.4 ± 0.8	0.956	8.7	6.36
C6	5.3 ± 0.2	0.988	14.9	3.44

the major transporter of copper and of Cu-complexes [53–55].

Human serum albumin contains only one tryptophan residue in its structure, Trp214, located in subdomain IIA, near Sudlow's drug binding site I [56]. This residue confers fluorescence emission to the protein upon excitation at 295 nm; it is very sensitive to its local environment, and its fluorescence emission easily responds to changes in the vicinity of the indole ring that may occur upon drugs' binding [56]. To evaluate the interaction of compounds **C1–C6** with HSA, solutions containing HSA were titrated with each complex, fluorescence emission spectra being measured upon each addition (see experimental part for details). For the Stern-Volmer analysis of data the emission at 340 nm was used and blank samples (in the absence of HSA) with the same concentration of the complexes were recorded and subtracted from each corresponding emission spectra. The effect of **C1–C6** in the HSA fluorescence emission is compared in Fig. 6.

The quenching was evaluated with the Stern-Volmer equation, allowing the determination of K_{SV} from the slope of the linear plot of I_0/I *vs.* [Q]. Knowing that the average lifetime for the Trp214 in HSA is $\tau_0 = 2.04 \times 10^{-9}$ s, under the experimental conditions used (this value was measured by us and details will be presented in a publication under preparation), the bimolecular constant, k_q, can be calculated for each complex using the relationship $k_q = K_{SV} / \tau_0$, and the accessibility of the fluorophore to the quencher evaluated [49].

Titration of HSA with **C1** yields a linear relationship in the Stern-Volmer plot (see Fig. 7), the $k_q = 3.08 \times 10^{13}\ M^{-1}\ s^{-1}$ value being larger than the limiting diffusion constant of the biomolecules ($K_{dif} = 2.0 \times 10^{10}\ M^{-1}\ s^{-1}$) [49], indicating that the fluorescence quenching is consistent with a static mechanism [57]. Assuming that a complex is formed between the compound and albumin, employment of the Scatchard equation enables the determination of the binding constant and the number of binding sites for this system. Results are included in Table 6.

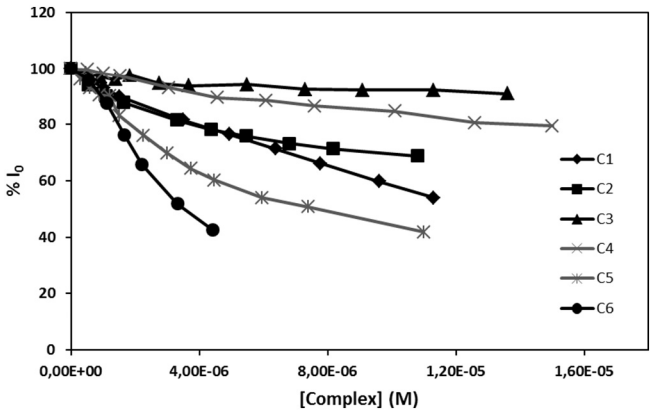

Fig. 6. Effect of complexes **C1–C6** in HSA fluorescence emission. Relative fluorescence intensity (%) at emission maxima with increasing complexes' concentration. λ_{ex} = 295 nm and λ_{em} = 340 nm.

Similarly to that observed with the system TO-*ct*DNA, complex **C3**, containing the methoxy derivative, was unable to quench the fluorescence of albumin (see SI section), meaning that this complex does not bind to the protein, at least in a way affecting the fluorescence of the Trp214 residue. The determination of the parameters for all other Cu (II)-compounds is detailed in the SI section and the values are included in Table 6.

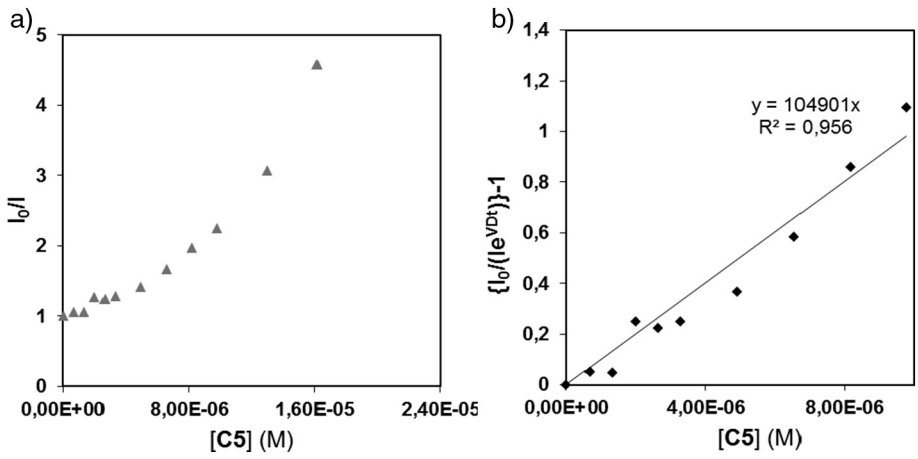

Fig. 5. a) Stern-Volmer plot at 530 nm for the fluorescence quenching of TO-*ct*DNA with increasing concentration of **C5** (0–16 μM). (I_0/I data were corrected for reabsorption and inner-filter-effects). b) Modified Stern-Volmer plot at 530 nm for the fluorescence quenching of TO-*ct*DNA with increasing concentrations of **C5**, considering both dynamic and static quenching mechanisms.

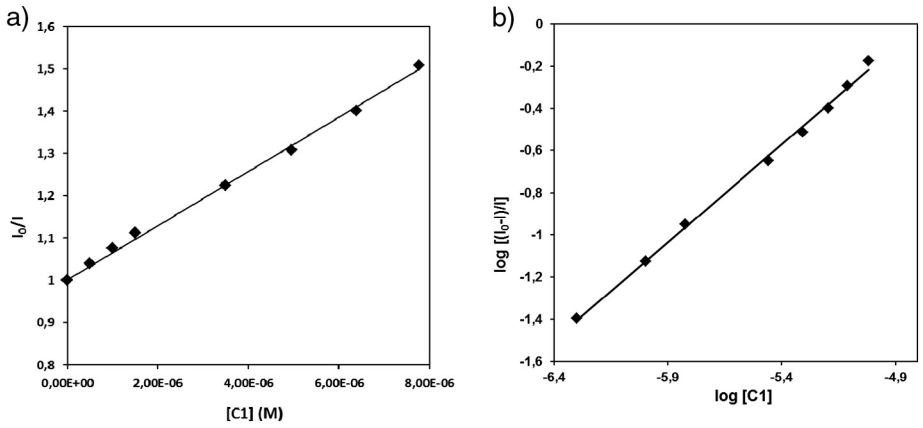

Fig. 7. a) Stern-Volmer plot at 339 nm obtained from steady-state (I_0/I) measurements for **C1** (0–7.78 μM) — [HSA] ~ 1.5 μM, and λ_{ex} = 295 nm (I_0/I data were corrected for reabsorption and inner-filter-effects). b) Scatchard plot at 339 nm obtained from steady-state (I_0/I) measurements for **C1** (0–7.78 μM) — [HSA] ~ 1.5 μM, and λ_{ex} = 295 nm, obtaining n = (0.93 ± 0.02) and log k = (4.44 ± 0.11).

The bimolecular constants [between (1.08 and 15.6) × 10^{13} M^{-1} cm^{-1}] support a static mechanism and the results clearly show that **C6** presents an HSA binding affinity much larger than any of the other complexes. Additionally, the constants for **C5** (log k = 4.94 ± 0.18) are higher than those obtained for **C1–C4**, showing the importance of the aromatic delocalization, suggesting that the π–π interactions play an important role in this process. For the Cu(II) complexes with smaller aromatic systems, **C1**, the complex derived from pyridoxal stands out, showing values for k_q and log K comparable to those of **C5**.

3.5.3. Cytotoxicity in human tumour cell lines

The cytotoxicity of the complexes **C1–C6** and the respective ligands **L1–L6** was evaluated using the MTT assay on PC3 prostate and MCF7 breast human cancer cells. The IC_{50} values were determined and are presented in Table 7 and Fig. S22.

In general, the anti-cancer activity of **C1–C4**, as judged from the measured IC_{50} values (Table 7), are modest. Noteworthy, the obtained IC_{50} values show that the presence of larger aromatic π-systems strongly favours the anti-proliferative ability in both cell lines. It is notorious the difference between the values retrieved for **C1–C4**, containing only one aromatic ring in the respective ligand, and those obtained for **C5** and **C6**, both with naphthalene derivatives. These compounds present IC_{50} values far lower than *cisplatin* (PC3 48 h, IC_{50} = 57.3 ± 14; MCF7 72 h, IC_{50} = 28 ± 6) [39]. The presence of an aromatic substituent at the pyrazole ring appears to have an effect in the PC3 cells but not in the MCF7 cells, as can be observed by the IC_{50} values obtained for **C5**, unsubstituted pyrazole, and **C6**, with a pyridine ring substituent at the pyrazole nitrogen (Table 7). **C1**, a pyridoxal-containing complex, which showed good water solubility, and moderate nuclease activity in the cleavage of plasmid DNA (see SI), was practically inactive in both tested cancer cell lines.

The results also revealed that the complexes exhibit higher cytotoxicity when compared to the ligands. The ligands **L1** and **L3** were found to be the less cytotoxic among the others (IC_{50} > 100 μM), while ligands **L5** and **L6** showed considerably low IC_{50} values, in particular in the MCF7 cells (Fig. S22). Upon coordination of **L5** and **L6** to copper(II), a considerable decrease in the IC_{50} was observed in the PC3 cells. This represented a very interesting result taking into consideration that this particular cancer cell line (androgen-independent prostate cells) has been described as resistant to chemotherapeutic regimen.

Table 7
In vitro cytotoxicity measured as the half-inhibitory concentration (IC_{50}) after 48 h incubation period for **C1–C6**, against prostate PC3 and breast MCF7 cancer cells. IC_{50} values reported in μM (± SD). (SD = standard deviation).

IC_{50} (μM)	48 h	
Compounds	PC3	MCF7
C1	> 100	> 100
C2	42.4 ± 10.8	80.2 ± 14.5
C3	> 100	48.1 ± 9.85
C4	> 100	49.5 ± 12.6
C5	7.71 ± 2.51	2.58 ± 0.63
C6	2.61 ± 1.45	2.65 ± 0.87

3.5.4. Apoptotic activity

In an attempt to study the mechanism of cell death, the effect in the PC3 cells of the most active complexes **C5** and **C6** on the activation of caspases 3/7 was evaluated. After 48 h treatment at a concentration equivalent to their IC_{50} values no induction of caspase-3/7 activation was observed when compared to the untreated cells (controls) (Fig. 8). Results revealed that **C5** and **C6** with high cytotoxicity in PC3 cells could probably induce cell death by other mechanisms than apoptosis.

3.5.5. Cu uptake by PC3 cells

The uptake of compound **C6** by PC3 cells was examined using nuclear microscopy. The typical ovoid appearance of the cells with a condensed central nucleus is consistent with the mass density (mass) images, and elemental distribution maps of P, K and Ca were obtained as depicted in Fig. 9. In control PC3 cells, the presence of Cu was vestigial (Fig. 9A). The PC3 cells incubated with **C6** at 20 μM and 200 μM for 24 h showed a relatively uneven Cu spatial distribution with

Table 6
Results for HSA binding studies with the synthesized complexes.

	C1	C2	C3	C4	C5	C6
K_{SV} × 10^5 (M^{-1})	0.63 ± 0.01	0.56 ± 0.04	n.a.	0.22 ± 0.01	1.30 ± 0.04	3.17 ± 0.23
k_q × 10^{13} (M^{-1} s^{-1})	3.08	2.73	n.a.	1.08	6.39	15.6
R^2	0.998	0.976	–	0.978	0.991	0.974
log K	4.44 ± 0.11	2.88 ± 0.09	n.a.	3.06 ± 0.24	4.94 ± 0.18	9.18 ± 0.30
n	0.93 ± 0.02	0.64 ± 0.02	n.a.	0.76 ± 0.05	0.96 ± 0.03	1.68 ± 0.05
R^2	0.997	0.996	–	0.981	0.993	0.996

n.a. means that no activity was recorded.

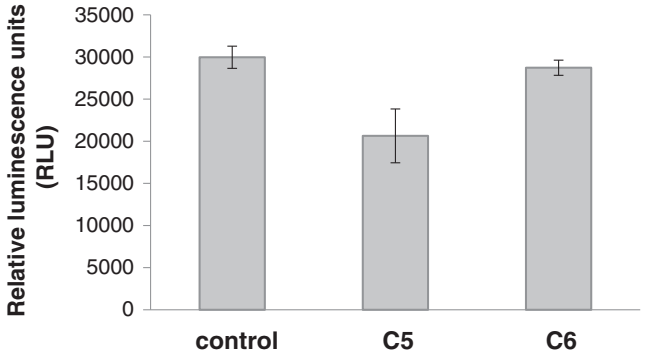

Fig. 8. Effect of complexes **C5** and **C6** on caspase 3/7 in human PC3 prostate cancer cells, after 48 h treatment at a concentration equivalent to their IC_{50} values.

a preferential localization in nuclear and perinuclear regions (Fig. 9B and C).

Quantitative elemental analysis of PC3 cells showed that intracellular Cu increased with **C6** concentration. PC3 cells treated with 20 μM **C6** had an average concentration of Cu of 340 ± 150 μg/g (dry weight), which further increased to 900 ± 500 μg/g (dry weight) in cells treated with 200 μM **C6**. The Cu concentration in control PC3 cells was vestigial, below 20 μg/g (dry weight). Therefore, it can be deduced that Cu levels in PC3 cells is correlated with the **C6** complex concentration.

The intracellular Cu increase in treated PC3 cells was accompanied with changes in the concentrations of physiologically relevant elements such as P, K and Ca in both nuclear and perinuclear regions. The average Ca concentration in cells increased with **C6** concentration (controls: 36 ± 6 μg/g; 20 μM **C6**: 130 ± 30 μg/g; 200 μM **C6**: 300 ± 70 μg/g). A 3-fold increase in P in 20 μM **C6** treated cells (1.7 ± 0.6 mg/g *versus* 0.5–0.8 mg/g range in control and 200 μM **C6**) and K in 200 μM **C6** treated cells (1.6 ± 0.4 mg/g *versus* 0.4–0.8 mg/g range in control and 200 μM **C6**) was also observed. In addition, PC3 cells treated with 200 μM **C6** deviated from the spheroid morphology and were smaller (see Fig. 9 C).

Results indicated disturbed homeostasis upon incubation with **C6** with an increase of important physiological elements such as P, K and Ca. This effect could be a consequence of complex modulation of transmembranar transporters that regulate Ca^{2+} and K^{+} ion fluxes [58]. This mechanism is in agreement with others recently reported indicating that blocking the activity of certain ion channels could have importance for anticancer therapy and hence opens a new field for anticancer drug research [59]. However, further investigations are needed for understanding the contribution of specific channels for this type of complexes.

4. Conclusions

In this work six new Schiff-base ligands derived from 5-methyl-1H-pyrazole-3-carbohydrazide and different aldehydes, namely pyridoxal (**L1**), salicylaldehyde and derivatives (**L2–L4**) and 2-hydroxynaphthene-1-carbaldehyde (**L5–L6**) were synthesized by condensation reactions, and fully characterized by analytical techniques. The Cu(II)-compounds **C1–C6** were synthesized by stirring methanolic solutions of the corresponding **L5–L6** and $CuCl_2.2H_2O$. The complexes were characterized by elemental analysis and spectroscopic techniques in order to prove their structural formulae. It was possible to assign a 1:1 relationship between metal ion and ligand, and square-based geometries with d_{x2-y2} ground state.

Compounds **C1–C6** were screened in biological studies, namely the evaluation of DNA and HSA binding ability, nuclease activity and cytotoxicity. Their anti-oxidant potential was evaluated in a DPPH assay, however, none of them (or the corresponding ligands) showed relevant anti-oxidant activity.

Although some of the complexes were able to bind *ct*DNA, only **C1** showed nuclease activity towards plasmid DNA. The displacement assays carried out with thiazole orange showed that complexes with larger delocalized π-systems, such as **C5** and **C6**, were able to partially intercalate into DNA in a greater extension than complexes with smaller aromatic systems, thanks to their planarity and ability to participate in π–π interactions.

It was also possible to prove that larger aromatic systems favor the interaction with HSA, as shown by fluorescence quenching titrations. However, **C1** and **C2** also showed HSA binding ability, contrary to **C3** and **C4**, which probably relates to the absence of electronegative groups in the *orto*-position to the coordinated phenolate. It can thus be assumed that HSA can serve as a carrier for these complexes, providing both transport to cellular targets and protection against clearance routes.

The cytotoxicity assays demonstrated the much higher activity of the compounds with larger delocalized π-systems, namely compounds **C5** and **C6**, which showed much better performance than those with smaller aromatic ligands. It can also be concluded that the effect of the ligands and the corresponding Cu(II)-complexes depends not only on

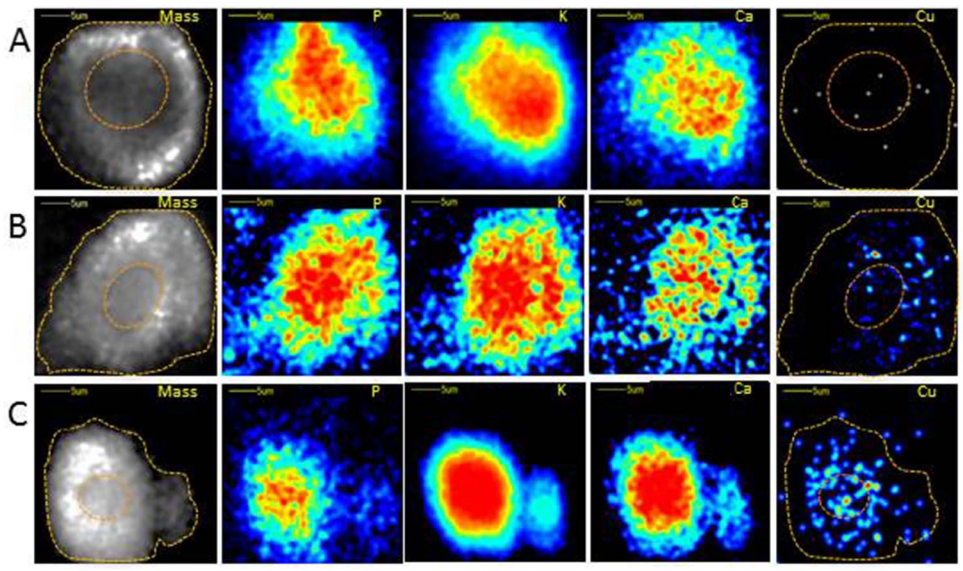

Fig. 9. Mass density (mass) and elemental maps of spatial distribution of P, K and Cu in individual PC3 cells under control (A), 20 μM (B) and 200 μM (C) of complex **C6** conditions. The dotted lines in mass and Cu maps indicate the cell contour and nuclear region. The mass density and elemental distributions are represented by a colour gradient with a dynamic scale: high level — black/red, to low level — white/dark blue.

the specific features in the auxiliary ligand and the metal ion, but also on the type of cancer cells.

Overall, this work demonstrated the high affinity that pyrazolyl derived Schiff bases **L1–L6** have to coordinate metal ions, namely Cu (II), forming stable complexes suitable for biological studies. It was proven that larger aromatic delocalized π-systems in such ligands provide more efficient complexes, both in the interaction assays with biomolecules such as DNA and HSA, and in the cytotoxic action. Moreover, the presence of an aromatic substituent at the pyrazole ring seems to enhance the cytotoxicity against cancer cells. Compounds **C5** and **C6**, not presenting relevant nuclease activity or radical scavenger potential, may have higher ability to interact/cross the cell membrane and accumulate in the nuclear/perinuclear region, in particular **C6**. The imbalance in the physiological elements involved in membrane potential and cellular homeostasis is therefore in line with the cytotoxicity of **C6** described above.

Acknowledgements

This work was supported by Fundação para a Ciência e Tecnologia (FCT) (projects UID/QUI/00100/2013, UID/MULTI/04349/2013, UID/BIO/04565/2013, RECI/QEQ-QIN/0189/2012, RECI/QEQ-MED/0330/2012), Programa Operacional Regional de Lisboa (LISBOA-01-0145-FEDER-007317) and programme Investigador FCT. The Portuguese NMR and Mass Spectrometry IST–UL Centers are acknowledged for the access to the equipment. The authors thank Fernando Pavan and Débora Leite de Campos for the Anti-*Mycobacterium Tuberculosis* studies.

Appendix A. Supplementary data

Supplementary data to this article can be found online at http://dx.doi.org/10.1016/j.jinorgbio.2017.05.011.

References

[1] C.-H. Zhou, H.-Z. Zhang, S.-F. Cui, J.-S. Lv, C.-Y. Yan, K. Wan, Y.-Y. Zhang, S.-L. Zhang, G.-X. Cai, R.-X. Geng, G.L.V. Damu, M. Prudhomme (Ed.), Advances in Anticancer Agents in Medicinal Chemistry, 2 Bentham e-Books, 2013, pp. 46–129.
[2] H. Khalil, M. Heulot, D. Barras, R. Jastrab, B. Tylkowski (Eds.), New Generation Bioinorganic Complexes, Walter de Gruyter GmbH, Berlin/Boston, 2016, pp. 143–159.
[3] B. Rosenberg, L. Vancamp, J.E. Trosko, V.H. Mansour, Nature 222 (1969) 385–391.
[4] S.J. Tan, Y.K. Yan, P.P.F. Lee, K.H. Lim, Future Med. Chem. 2 (2010) 1591–1608.
[5] C. Santini, M. Pellei, V. Gandin, M. Porchia, F. Tisato, C. Marzano, Chem. Rev. 114 (2014) 815–862.
[6] J. Osredkar, N. Sustar, J. Clin. Toxicol. S3 (2011) 001.
[7] Z.C. Liu, B.D. Wang, B. Li, Q. Wang, Z.Y. Yang, T.R. Li, Y. Li, Eur. J. Med. Chem. 45 (2010) 5353–5361.
[8] C.M. da Silva, D.L. da Silva, L.V. Modolo, R.B. Alves, M.A. de Resende, C.V.B. Martins, Â. de Fátima, J. Adv. Res. 2 (2011) 1–8.
[9] L.-X. Cheng, J.-J. Tang, H. Luo, X.-L. Jin, F. Dai, J. Yang, Y.-P. Qian, X.-Z. Li, B. Zhou, Bioorg. Med. Chem. Lett. 20 (2010) 2417–2420.
[10] Q.M. Hasi, Y. Fan, X.Q. Yao, D.C. Hu, J.C. Liu, Polyhedron 109 (2016) 75–80.
[11] Z.-Y. Ma, X. Qiao, C.-Z. Xie, J. Shao, J.-Y. Xu, Z.-Y. Qiang, J.-S. Lou, J. Inorg. Biochem. 117 (2012) 1–9.
[12] X.Q. Zhou, Y. Li, D.Y. Zhang, Y. Nie, Z.J. Li, W. Gu, X. Liu, J.L. Tian, S.P. Yan, Eur. J. Med. Chem. 114 (2016) 244–256.
[13] S.G. Kucukguzel, S. Senkardes, Eur. J. Med. Chem. 97 (2015) 786–815.
[14] F.K. Keter, J. Darkwa, Biometals 25 (2012) 9–21.
[15] A. Dias, R.R.S. Salvador, Pharmaceuticals 5 (2012) 317–324.
[16] T.N. Mandal, S. Roy, A.K. Barik, S. Gupta, R.J. Butcher, S.K. Kar, Polyhedron 7 (2008) 3267–3274.
[17] G.M. Sheldrick, SADABS, Version 2.10, University of Göttingen, Germany, 2004.
[18] O.V. Dolomanov, L.J. Bourhis, R.J. Gildea, J.A.K. Howard, H. Puschmann, J. Appl. Crystallogr. 42 (2009) 339–341.
[19] G.M. Sheldrick, Acta Crystallogr. Sect. A 64 (2008) 112–122.
[20] G.M. Sheldrick, Acta Crystallogr. Sect. C 71 (2015) 3–8.
[21] J.M. Teare, R. Islam, R. Flanagan, S. Gallagher, M.G. Davies, C. Grabau, BioTechniques 22 (1997) 1170–1174.
[22] S.R. Gallagher, F.A. Ausubel, R. Brent, R.E. Kingston, D.D. Moore, J.G. Seidman, J.A. Smith, K. Struhl (Eds.), Current Protocols in Molecular Biology, John Wiley & Sons, New York, 1989.
[23] D.G. Fasman, Practical Handbook of Biochemistry and Molecular Biology, CRC Press, Boston, 1992.
[24] M.B. Fisher, S.J. Thompson, V. Ribeiro, M.C. Lechner, A.E. Rettie, Arch. Biochem. Biophys. 356 (1998) 63–70.
[25] A. Coutinho, M. Prieto, J. Chem. Educ. 70 (1993) 425–428.
[26] J.T. Marques, R.F.M. de Almeida, J. Chem. Educ. 90 (2013) 1522–1527.
[27] A. Verissimo, L.C. Alves, P. Filipe, J.N. Silva, R. Silva, M.D. Ynsa, E. Gontier, P. Moretto, J. Pallon, T. Pinheiro, Microsc. Res. Tech. 70 (2007) 302–309.
[28] G.W. Grime, M. Dawson, Nucl. Instrum. Methods B 104 (1995) 107–113.
[29] M.S.e.a. Vasco, J. Microsc. (2017).
[30] R.M. Godinho, M.T. Cabrita, L.C. Alves, T. Pinheiro, Metallomics 6 (2014) 1626–1631.
[31] Y. Xia, C.D. Fan, B.X. Zhao, J. Zhao, D.S. Shin, J.Y. Miao, Eur. J. Med. Chem. 43 (2008) 2347–2353.
[32] J. Clayden, N. Greeves, S. Warren, P. Wothers, Organic Chemistry, 1st ed., Oxford University Press, Oxford, 2001.
[33] T. Rosu, E. Pahontu, M. Reka-Stefana, D.C. Ilies, R. Georgescu, S. Shova, A. Gulea, Polyhedron 31 (2012) 352–360.
[34] K. Nakamoto Infrared and Raman Spectra of Inorganic Compounds, Wiley, 5th ed.
[35] T. Mukherjee, J.C. Pessoa, A. Kumar, A.R. Sarkar, Inorg. Chim. Acta 426 (2015) 150–159.
[36] D.F. Back, G.M. de Oliveira, L.A. Fontana, B.F. Ramao, D. Roman, B.A. Iglesias, J. Mol. Struct. 1100 (2015) 264–271.
[37] I. Correia, J.C. Pessoa, M.T. Duarte, M.F.M. da Piedade, T. Jackush, T. Kiss, M.M.C.A. Castro, C.F.G.C. Geraldes, F. Avecilla, Eur. J. Inorg. Chem. (2005) 732–744.
[38] I. Correia, S. Roy, C.P. Matos, S. Borovic, N. Butenko, I. Cavaco, F. Marques, J. Lorenzo, A. Rodriguez, V. Moreno, J.C. Pessoa, J. Inorg. Biochem. 147 (2015) 134–146.
[39] J.C. Pessoa, M.J. Calhorda, I. Cavaco, P.J. Costa, I. Correia, D. Costa, L.F. Vilas-Boas, V. Felix, R.D. Gillard, R.T. Henriques, R. Wiggins, Dalton Trans. (2004) 2855–2866.
[40] S. Konar, A. Jana, K. Das, S. Ray, S. Chatterjee, J.A. Golen, A.L. Rheingold, S.K. Kar, Polyhedron 30 (2011) 2801–2808.
[41] J.C. Pessoa, I. Cavaco, I. Correia, I. Tomaz, P. Adao, I. Vale, V. Ribeiro, M.M.C.A. Castro, C.C.F.G. Geraldes, ACS Symp. Ser. 974 (2007) 340–351.
[42] K. Das, T.N. Mandal, S. Roy, S. Gupta, A.K. Barik, P. Mitra, A.L. Rheingold, S.K. Kar, Polyhedron 29 (2010) 2892–2899.
[43] A. Rockenbauer, L. Korecz, Appl. Magn. Reson. 10 (1996) 29–43.
[44] A. Sreekanth, M.R.P. Kurup, Polyhedron 22 (2003) 3321–3332.
[45] J. Peisach, W.E. Blumberg, Arch. Biochem. Biophys. 165 (1974) 691–708.
[46] U. Sakaguchi, A.W. Addison, J. Chem. Soc. Dalton Trans. (1979) 600–608.
[47] O.P. Sharma, T.K. Bhat, Food Chem. 113 (2009) 1202–1205.
[48] S. Satyanarayana, J.C. Dabrowiak, J.B. Chaires, Biochemistry 32 (1993) 2573–2584.
[49] W.R. Lakowicz, Principles of Fluorescence Spectroscopy, 3rd ed., Springer, 2006.
[50] J. Nygren, N. Svanvik, M. Kubista, Biopolymers 46 (1998) 39–51.
[51] N. Seedher, P. Agarwal, J. Lumin. 130 (2010) 1841–1848.
[52] N.E. Hellman, J.D. Gitlin, Annu. Rev. Nutr. 22 (2002) 439–458.
[53] W. Bal, J. Christodoulou, P.J. Sadler, A. Tucker, J. Inorg. Biochem. 70 (1998) 33–39.
[54] Y. Gou, J.X. Qi, J.P. Ajayi, Y. Zhang, Z.P. Zhou, X.Y. Wu, F. Yang, H. Liang, Mol. Pharm. 12 (2015) 3597–3609.
[55] D. Sanna, P. Buglyo, A.I. Tomaz, J.C. Pessoa, S. Borovic, G. Micera, E. Garribba, Dalton Trans. 41 (2012) 12824–12838.
[56] G. Sudlow, D.J. Birkett, D.N. Wade, Mol. Pharmacol. 12 (1976) 1052–1061.
[57] S. Tabassum, M. Ahmad, M. Afzal, M. Zaki, P.K. Bharadwaj, J. Photochem. Photobiol. B Biol. 140 (2014) 321–331.
[58] J.L. Wedding, H.H. Harris, C.A. Bader, S.E. Plush, R. Mak, M. Massi, D.A. Brooks, B. Lai, S. Vogt, M.V. Werrett, P.V. Simpson, B.W. Skelton, S. Stagni, Metallomics (2017), http://dx.doi.org/10.1039/C6MT00243A.
[59] A. Arcangeli, A. Becchetti, Pharmaceuticals, (2010), pp. 1202–1224.